Fall 12-16-2016

Effect of Small-Scale Continental Shelf Bathymetry on Storm Surge Generation

Sunni A. Siqueira
University of New Orleans, piratepheasant@gmail.com

Effect of Small-Scale Continental Shelf Bathymetry on Storm Surge Generation

A Thesis

Submitted to the Graduate Faculty of the
University of New Orleans
in partial fulfillment of the
requirements for the degree of

Master of Science
in
Applied Physics

by

Sunni Ann Siqueira

B.S. University of New Orleans, 2012

December, 2016

Table of Contents

List of Figures

List of Tables

ABSTRACT

Idealized bathymetries were subjected to idealized cyclones in order to measure the storm surge response to a range of bathymetry features, under various storm conditions. Ten bathymetries were considered, including eight shoals, one pit, and a featureless reference domain. Six storms (two different sizes/intensities and three different landfall directions) were used as meteorological forcing. The bathymetry features influenced local surge response during pre- and post-peak surge conditions. However, peak surge and surge at the coast were not meaningfully affected by the presence of the bathymetry features considered. The effect of three bathymetry feature parameters on surge response was analyzed (i.e. depth below mean sea level, cross-shore width, and distance from shore). Of these parameters, feature depth below mean sea level was the most influential on surge generation.

storm surge; bathymetry; ADCIRC

1. Introduction

1.1. Background

Simulating oceanographic processes requires specification of ocean depths (bathymetry). Techniques for collecting these data have significantly improved in recent years due to the development of multibeam echo sounders and remote sensing technology, such as LiDAR, allowing for much higher resolution. Increasing resolution of bathymetric data sets necessitates increased storage and data transmission requirements. Additionally, it is more difficult to process and manipulate large data sets than small ones with regard to computer memory requirements. Therefore, it is desirable to reduce the size of the data set through thinning while maintaining fidelity to the surface being represented. The process of thinning removes redundant bathymetric information, which in the case of oceanographic modeling is any bathymetry data that is not necessary to fully represent the processes being modeled. To develop thinning criteria, we must understand the effect of bathymetric features on simulated phenomena. This process begins by considering storm surge generation on the continental shelf.

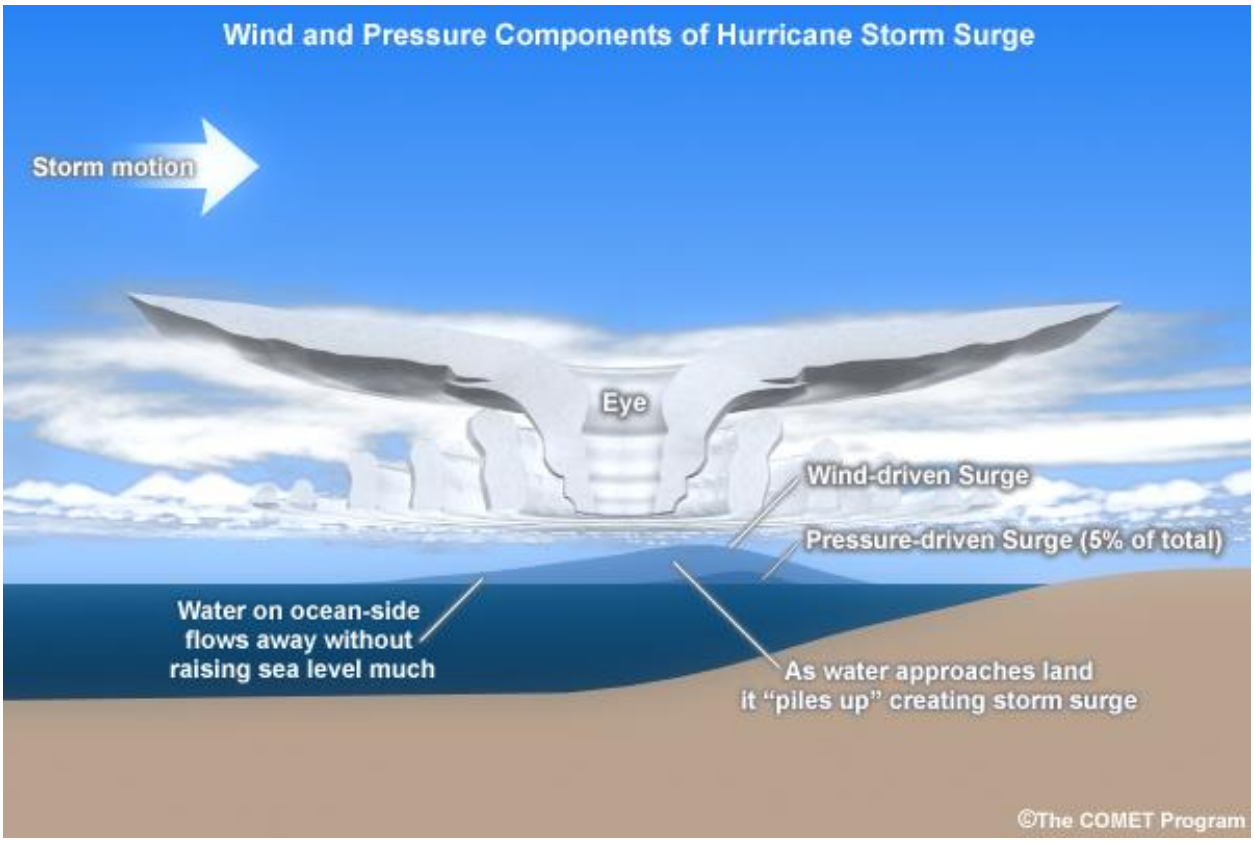

Figure 1-1: Wind and pressure components of hurricane storm surge. As the storm moves towards land (from left to right), friction between the wind and the water allows the water to be pushed in the direction of the wind's motion. This cross section of the storm and the continental shelf shows the inverse relationship between surge generation and water depth. (Retrieved October 11, 2016, from http://www.nhc.noaa.gov/surge/.)

Storm surge is a change in sea level accompanying a hurricane or other intense storm, whose height is the difference between the sea surface's observed level and the level that would have occurred in the absence of the storm. During a hurricane, storm surge is produced by water being pushed toward the shore by the force of the winds moving cyclonically around the area of low pressure located at the center of the storm (Figure 1-1). Friction between the wind and the water allows the water to be pushed in the direction of the wind's motion. The low pressure of the storm system contributes to increased sea surface elevation, this is known as the inverted barometer effect; however, the impact on surge of the low pressure is minimal in comparison to the water being forced toward the shore by the wind. Tides and surface waves also contribute to the sea surface elevation and can magnify surge elevations, but their effects are not included in this study.

The geometry of the continental shelf is another important factor influencing storm surge. In shallow water the slope the water surface must take to balance the force of the cross-shelf winds is inversely proportional to the depth of the water (Pugh, 1996). This relationship is due to the fact that the force of the winds is acting on a smaller volume of water in a shallow area than in an equal area of deep water. Wide, shallow shelves experience greater storm surge than narrow or steeply sloping shelves under the same storm conditions. Wide shelves experience greater surge because there is a larger distance over which surge can be generated, and since surge is inversely proportional to water depth (and to bottom slope), shallow shelves generate more surge than deep or steeply sloping shelves. Since the generation of surge is sensitive to water depth, the geometry of smaller scale features on the continental shelf, such as shoals and pits may, also influence surge. It is the goal of this study to determine such features' influence on storm surge generation.

1.2. Review of Literature

Considerable research has been undertaken to understand various influences on the generation of storm surge in the coastal zone (Blain et al., 1994; Irish et al., 2008; Rego and Li, 2009; Weaver and Slinn, 2010; and Li et al., 2013). To date, these influences can be divided into two categories: 1) storm parameters such as wind intensity, storm size, translation speed, landfall direction, and arrival relative to tidal phase, and 2) physical characteristics of the environment, for example, continental shelf slope, width, and features. The following sections summarize the current understanding of how these various parameters affect the generation of storm surge in coastal waters.

1.2.1. Storm Parameters

Hurricanes are characterized by several defining characteristics, their intensity measured as wind speed, their size as a function of the radius to the band of winds having maximum speed (R_m), and their translation speed. Surge generation is also affected by the direction of the storm's approach to land, as well as its arrival relative to the tidal phase. The breakdown of each hurricane parameter and its influence on surge generation is presented.

1.2.1.1. Wind Intensity

The role of hurricane wind intensity on surge generation was examined by Irish et al. (2008), Rego and Li (2009), and Li et al. (2013). Irish et al. (2008) note that although wind intensity, as measured by the Saffir-Simpson scale (Simpson and Saffir, 1974), is a good

predictor of the wind damage expected by a hurricane, it alone is not the best predictor of storm surge. This is particularly true in the case of intense storms on mildly sloping continental shelves because surge generation is proportional to the square of the wind velocity as well as inversely proportional to the bottom slope. Rego and Li (2009) found that increasing wind intensity results in the increase of both flooded volumes and peak surge elevation. They also discovered that wind intensity has a more significant impact on peak surges as compared to the R_m. While testing the sensitivity of peak surge to domain size under differing storm intensities, Li et al. (2013) showed that with other parameters fixed, an increase in storm intensity causes an increase in peak surge.

1.2.1.2. Storm Size

Irish et al. (2008), Rego and Li (2009), and Li et al. (2013) also considered the influence of storm size on surge generation. Irish et al. (2008) found that for a given storm intensity, peak surge increases with increasing R_m. This relationship holds for all bottom slopes. Their numerical results indicate that the role of storm size in surge generation becomes much more important on mildly sloping bottoms and for intense storms. Surge generation is inversely proportional to bottom slope and proportional to wind stress, and a larger storm increases the fetch and duration over which winds can act. Historical observations were also used to support these findings. Rego and Li (2009) found that similar to increasing wind intensity, increasing a storm's R_m results in the increase of both flooded volumes and peak surge elevation. In keeping with the results of Irish et al. (2008), Li et al. (2013) found that peak surge increases with increasing R_m.

1.2.1.3. Translation Speed

Irish et al. (2008), Rego and Li (2009), and Li et al. (2013) investigated the influence of hurricane translation speed on peak surge. The results of Irish et al. (2008) indicate a correlation between storm translation speed (values from 2.6 to 10.2 m s^{-1}) and peak storm surge for steep to moderate bottom slopes. When the bottom slope is ≤ 1:2500, a 50% increase in forward speed translates to a 15%–20% increase in peak surge. Of the cases they investigated, only the case with the mildest bottom slope (1:10,000) did not experience an increase in peak elevation with increased translation speed. Rego and Li (2009) found that a hurricane's forward speed has significant positive effect on peak surge heights but a significant negative effect on total maximum flooded volumes. For example, a slower storm produces lower peak surges that travel far inland, whereas a faster hurricane will move rapidly across the shoreline generating higher surges but flooding a relatively narrower section of the coast. Li et al. (2013) found that peak surge increases with increasing hurricane translation speed for speeds less than 12 m s^{-1}, and it remains the same for forward speeds between 12 and 21 m s^{-1}.

1.2.1.4. Landfall Direction

Irish et al. (2008) and Li et al. (2013) tested the sensitivity of surge response to landfall direction. They both use idealized rectangular domains, but with different orientations (i.e., shore is located at the northern boundary of Irish et al.'s domain but at the western boundary of Li et al.'s domain). In both studies all landfalling hurricanes make landfall in the middle of the shore. For this discussion, storm tracks are described using positive angles in which θ is the angle rotating from the right side of the shoreline to the hurricane track in a clockwise direction (Figure 1-2), i.e., the shore normal track is 90°.

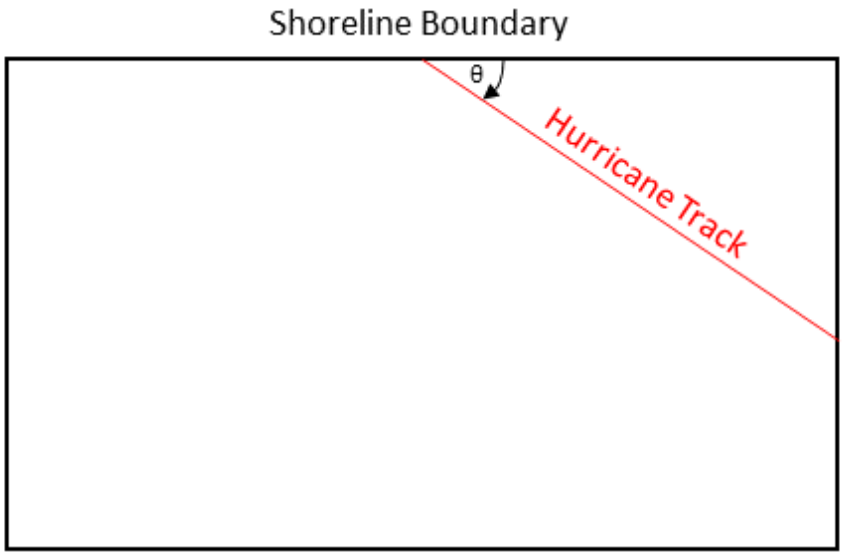

Figure 1-2: Convention for defining storm track angle. Storm tracks are described using positive angles in which θ is the angle rotating from the right side of the shoreline to the hurricane track in a clockwise direction.

Irish et al. found that all storm tracks with more westerly headings (45°-75°) produced smaller surges than the due north (90°) track for both moderately and mildly sloping bottoms. For the most mildly sloping bottom (1:10,000), storms with more easterly headings (105°-150°) produced surges that were as large, or slightly larger (no more than 8%), than the due north (90°) track. These results were for storms with a forward speed of 5.1 m s^{-1}. Li et al. conclude that landfall direction could affect simulated surge level dramatically, having a greater impact than R_m and translation speed. They tested twelve different storm tracks and found that peak surge was highest when a hurricane makes landfall with a 90° track (bottom slope 1:1,500).

1.2.1.5. Arrival Relative to Tidal Timing

As one might expect, Rego and Li (2009) confirmed that hurricanes landfalling at high tide yield both greater flooded volumes and peak surges than those landfalling at low tide. They considered the cases of double amplitude and normal amplitude tides with the storm landfalling at high and low tide for each of the tidal amplitudes. Variations are only about ±16% of the inundation volume of the simulation without tidal forcing. They also found that tide-surge nonlinearity decreases the impact of high- or low-tide landfalls. For example, peak storm tides for high tide and double high tide should be greater than the no tide case by about 0.33 and 0.66 m (the tidal amplitude), and they are not.

1.2.2. Domain Characteristics

The coastal zone can be described in terms of its regional bathymetry such as its continental shelf width and slope, as well as by its shoreline geometry and the presence of any local-scale features on the shelf. All of these characteristics can be expected to exert some influence on storm surge generation. Here the influence of regional bathymetry, positive and negative perturbations to the local bathymetry, and the size of the modeled domain on storm surge is presented.

1.2.2.1. Domain Size

Blain et al. (1994) compared hurricane storm surge generation in three domains of differing sizes, subject to two different open boundary forcings, in order to determine the influence of domain size on storm surge response. All of the domains had identical bathymetry and identical discretization in the areas they held in common. Much of the small (Florida coast) domain was on the continental shelf at depths of < 130 m, and its boundaries were almost exclusively across the continental shelf. The medium (Gulf of Mexico) domain contained the small domain and all surrounding regions in the Gulf of Mexico. It had two open ocean boundaries; one across the Strait of Florida and one across the Yucatan Channel. The large (Eastcoast) domain contained the medium domain and also included the western North Atlantic Ocean and the Caribbean Sea. Its open ocean boundary was the entire stretch of ocean along the 60° W meridian from Nova Scotia in the North to Venezuela in the South.

The small domain underestimated surge using both boundary condition specifications considered in the study and cannot be used to obtain a physically relevant storm surge response. This is because an appropriate elevation boundary condition cannot be specified at the cross-shelf boundaries because in order to do so, the storm surge generated on the shelf would need to be known in advance. The domain was also too small relative to the spatial scale of a hurricane. In the medium domain, the two open ocean boundaries significantly influenced the setup of modes in the Gulf of Mexico. The frequency of the modes varied with the application of different boundary conditions (i.e., it was highly sensitive to boundary condition specification), and this domain had shortcomings in the representation of basin to basin dynamics. The large domain was insensitive to boundary condition specification. Simulations using this domain give good results even without the elevation boundary condition being precisely known. It was much better at representing basin to basin dynamics, as evidenced by the more natural resonant modes in the Gulf of Mexico. In order to obtain the most realistic results, it is best for the open boundary to be far from the intricate processes that occur on the continental shelf and the within the basin in response to the hurricane.

Li et al. (2013) also show that simulated storm surge is significantly affected by domain size especially when the modeled domain is relatively small. In keeping with Blain et al. (1994), they found that peak surge is underestimated when the model domain used is too small. However, when the domain size is greater than a given threshold, they found that simulated storm surge is insensitive to domain size. One difference between the two studies is that Li et al. (2013) used rectangular idealized domains free from basin to basin interaction. Li et al. (2013) determined the threshold domain size for ranges of wind intensities, R_m, translation speeds, landfall directions, bottom slopes, and continental shelf widths. Their results indicate that this threshold domain size is not sensitive to storm intensity but increases linearly with increasing hurricane R_m. When a hurricane approaches land perpendicularly, the threshold domain size increases with increasing hurricane translation speed. Furthermore, the domain size requirement changes considerably as the hurricane landfall direction varies from shore normal. In considering bathymetric variations, threshold domain size decreases with increasing bottom slope, and the cross-shore size requirement increases with increasing continental shelf width for shelves < 100 km. Their findings provide a quantitative understanding of how domain size influences simulated peak surge under various hurricane and regional-scale bathymetry conditions.

1.2.2.2. Continental Shelf Slope

Irish et al. (2008), Weaver and Slinn (2010), and Li et al. (2013) consider the influence of continental shelf slope on storm surge generation. Irish et al. found that for a given storm, decreasing bottom slope results in increased peak surge. Relating to storm size, their parameter of interest, they discovered that the linear trend of increasing peak surge with increasing storm size becomes steeper as shelf slope becomes milder, implying that the role of storm size in producing surge becomes increasingly important over mildly sloping bottoms. When examining the combined influence of forward speed and bottom slope on surge generation, with the exception of their most mildly sloping bottom (1:10,000), increasing forward speed resulted in increasing surge with decreasing slope. Weaver and Slinn examined behavior of storm surge on slopes ranging from 1:20 to 1:200 in their 1D simulations. In these cases, the slopes extended 50 km offshore. To develop their baseline data set they generated surge predictions on the sloped profiles in the absence of any bathymetric perturbations. With all other factors held constant, they found that peak surge was inversely proportional to shelf slope. Li et al.'s results show that peak surge increases with decreasing bottom slope which corresponds to Irish et al.'s and Weaver and Slinn's findings. Additionally, they found that the required domain size decreases with increasing bottom slope.

1.2.2.3. Continental Shelf Width

Li et al. (2013) discovered that peak surge increases with increasing shelf width for shelves less than 100 km and is not sensitive to increases in shelf width beyond 100 km.

1.2.2.4. Perturbations to Local Bathymetry

Weaver and Slinn (2010) examined the extent to which variations in nearshore bathymetry affect the storm surge at the coast. They created a 1D idealized bathymetry which was altered by adding a local Gaussian disturbance at various distances from the shoreline. For each of the bottom slopes considered a suite of Gaussian disturbances was created. The perturbations were defined by their amplitudes (percentage of the local water depth), their widths (100 to 5000 m), and the distance from shore to their centers (500 to 5000 m). They found that storm surge at the coast varied only slightly as a consequence of local variation in the bathymetry, with the bulk of the simulations predicting the surge levels at the shore to be very close to that of the unperturbed bottom.

They found that the resulting surge varied by ±10% for amplitude variations that were less than ±40% of the initial bathymetry. Fluctuations up to +60% would generate a difference at the coast of at most +20%. As the perturbations' amplitudes become larger, they found that the cases of extreme width and proximity to the shoreline start to produce outliers in the results. Depending on the maximum acceptable root-mean-square deviation (RMSD) allowed, one can allow for a large range of bathymetric variations without significantly changing the surge results at the shoreline.

Weaver and Slinn (2010) also looked at the relative surge versus the width of the perturbation, finding that the wider disturbances generated a greater deviation from the unperturbed result, but they did not quantify this aspect of their findings. Also, as the center of the perturbation moves farther offshore, the relative depth increases depending on the average bottom slope. They discovered that there is a limit where, beyond that distance, the effects of

bathymetric fluctuations at the shore begin to diminish. They note that for all cases this limit coincides with a depth of about 30 m, and they call this the depth of relative influence (DRI). Seaward of that limit, the effects of altering the bathymetry on surge begin to diminish.

Two-dimensional simulations conducted by Weaver and Slinn (2010), in which they perturbed the bathymetry in locations affected by the historical storms used as forcing for those simulations, led to results that were consistent with their 1D findings.

1.3. Gaps in the Current Knowledge

Most of the recent studies considered (Irish et al., 2008; Weaver and Slinn, 2010; Li et al., 2013) considered factors affecting only peak surge generation or peak surge and inundation (Rego and Li, 2009). The study presented herein will address the complete time evolution of surge, with a focus on surge recession. With the exception of Weaver and Slinn, past focus has been on surge generation at the shoreline by considering surge generation offshore. In our study the focus is between 5 km and 70 km offshore. While Weaver and Slinn did examine the influence of bathymetric perturbations on surge generation, they only consider their influence on peak surge. In their 1-D simulations Weaver and Slinn made qualitative remarks about the influence of a bathymetric perturbation's cross-shore width and distance from shore on peak surge, quantifying only the influence of amplitude. The study herein extends this work by quantifying the influence of feature parameters (i.e., amplitude, cross-shore width, distance from shore) on the generation of storm surge. In the 2-D studies of Weaver and Slinn, perturbations to the local bathymetry are much smaller in area than the features considered in this study and have only ± 20% change in elevation to the surrounding bathymetry. The features considered in this study are larger, farther from shore, and on a more gently sloping continental shelf than the bathymetric perturbations that they used in their 2-D simulations. In their 2-D simulations, Weaver and Slinn do examine the perturbations' influence on local influence surge, not just at the shoreline, but only at peak elevation.

1.4. Purpose of this Study

It is the purpose of this study to determine the influence of continental shelf features on simulated storm surge considering various storm parameters. This will be accomplished through 1) the evaluation of which feature parameters (i.e., elevation, cross-shore width, and distance from shore) are the most influential on surge response, and 2) the examination of how the presence of continental shelf features alters the surge response subject to various storm parameters.

2. Methodology

2.1. Overview of Methodology

To determine the influence of offshore bathymetric features on storm surge, numerical simulations utilizing idealized domains and tropical cyclones were conducted. Additionally, the sensitivity of surge to storm landfall direction and to storm size was considered, both in the presence and absence of the bathymetric features. The next sections describe the design of the domains, including their features, the design of the storms, and provide a description of the storm surge simulator, ADCIRC. The analysis techniques are also discussed in detail.

2.2. Domain Design

2.2.1. Design of Regional-Scale Bathymetry

Each domain represents ocean depths from the shoreline, over the continental shelf and slope, and out into the deep ocean through the application of idealized geometries for each of the geomorphic components, the shoreline, continental shelf, continental slope, and the abyssal plain. Each domain is rectangular, with dimensions of 400 km alongshore and 300 km cross-shore. These dimensions exceed the threshold domain size needed to prevent underestimation of surge, as defined in Li et al. (2013), for the chosen continental shelf characteristics and storm parameters, as described below. Depth contours are shore-parallel (Irish et al., 2008; Li et al., 2013), and each region (i.e. shelf, slope, abyssal plain) has a constant slope. The continental shelf width is 100 km, which is the width at which peak surge becomes insensitive to increasing shelf width according to Li et al. (2013). Its slope is 0.0003, which is representative of the gently sloping shelves off the coasts of Louisiana (Irish et al., 2008). Depths over the shelf range from 0 to 30 m, which means that the entire continental shelf lies within the range of the depth of relative influence (DRI) defined by Weaver and Slinn (2010). The slope of the continental slope section is 0.04, which is the global average (Wefer, 2003), and its depths range from 30 to 2000 m. The depth of the abyssal plain for this application is set to 2000 m. The reference domain has no bathymetric feature on its continental shelf (featureless) and is of uniform depth in the alongshore dimension. Other domains are identical to the reference domain except at the location of their features.

2.2.2. Design of Local-Scale Bathymetry Features

Just as the large-scale geomorphic components were represented using idealized geometries, the bathymetry features on the continental shelf were also simulated using idealized geometries. The relief in the cross-shore direction was modeled using a Gaussian curve over an ellipse, and the alongshore edges were then smoothed using cosine-shaped curves. Three parameters (i.e. depth below mean sea level (MSL), cross-shore width, and distance from shore) were varied to arrive at eight unique, raised bathymetric features (shoals). The term raised indicates that a feature protrudes relative to the surrounding seafloor. It does not imply that a

feature is subaerial. A domain containing a depressed feature (pit) and a featureless reference domain were also constructed.

For this study, all features were 50 km long in the alongshore direction and located in the center of the domain with respect to the alongshore direction. Each shoal was defined by three parameters, 1) its distance from shore, either 25 or 50 km; 2) its cross-shore width, either 3.75 or 11.25 km; and 3) its depth relative to mean sea level (MSL), either 0.5 or 3 m below MSL. The combination of these parameters resulted in 8 unique raised features. A single depressed feature (pit) was considered. It had the dimensions and location of the most influential raised feature but an inverse amplitude (7 m below the surrounding seafloor rather than protruding 7 m above the surrounding seafloor).

Table 2-1 lists each domain considered in this study and provides a detailed description of their features, where applicable. With the exception of the reference domain, which has no bathymetry feature on its continental shelf, domains were named for their features. The domain name convention that is used throughout this document it as follows: FD is the featureless reference domain, S indicates shoal, P indicates pit; 25 or 50 indicates feature distance (km) from shore; W indicates the wider, 11.25 km features; and -Sh indicates the shallower features that are 0.5 m below mean sea level (MSL). For example, S50W-Sh, indicates the domain has a shoal 50 km from shore with the wider (11.25 km) width and the shallower (0.5 m) depth below MSL. A second example, S25, indicates the domain has a shoal centered 25 km from shore with the narrower (3.75 km) width and the deeper (3.0 m) depth below MSL.

Table 2-1: Model domains considered in this study with descriptions of their features, if applicable.

Feature/ Domain Name	Distance from Shore (km)	Cross-Shore Width at Seafloor (km)	Depth below MSL (m)	Depth Relative to Surrounding Seafloor (m)
S25	25	3.75	3	4.5
S25-Sh	25	3.75	0.5	7
S25W	25	11.25	3	4.5
S25W-Sh	25	11.25	0.5	7
S50	50	3.75	3	12
S50-Sh	50	3.75	0.5	14.5
S50W	50	11.25	3	12
S50WSh	50	11.25	0.5	14.5
P	25	11.25	14.5	-7
FD	NA	NA	NA	0

Figure 2-1 depicts the 400 by 300 km domain in plan-view, showing the locations and widths of the features chosen for this study. The location of the continental shelf break is also shown. The alternative values of two of the parameters that were varied (feature distance from shore and cross-shore width) are clearly visible in Figure 2-1. The alternative values of feature depth below MSL are shown in Figure 2-2.

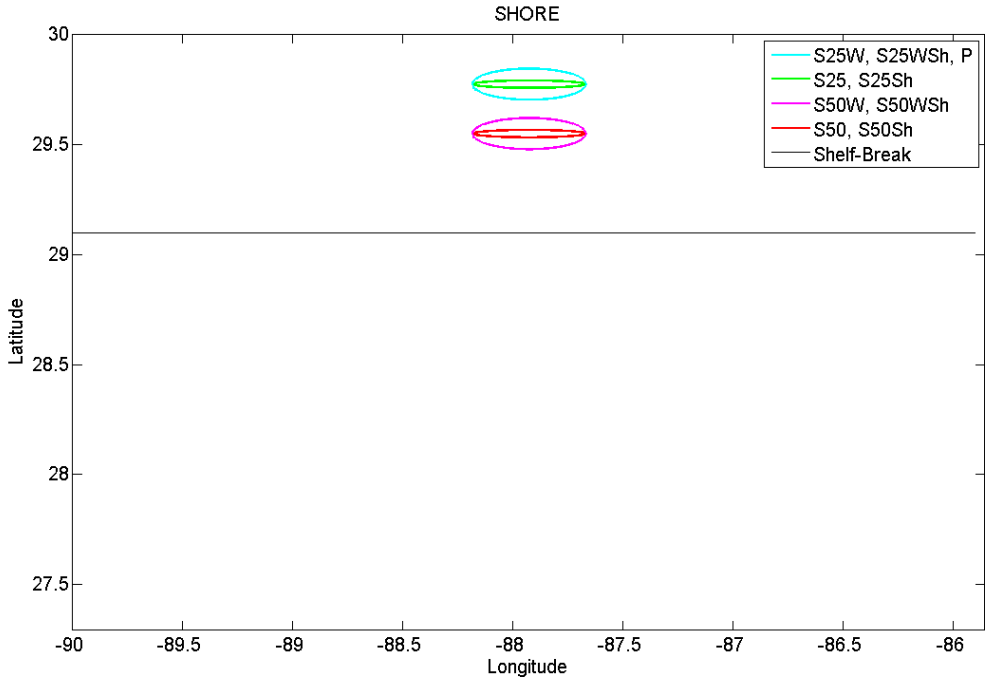

Figure 2-1: Plan-view diagram of the 400 by 300 km domain showing feature placement at 25 and 50 km from shore and the location of the continental shelf break 100 km from shore. The two possible feature widths are shown at each location.

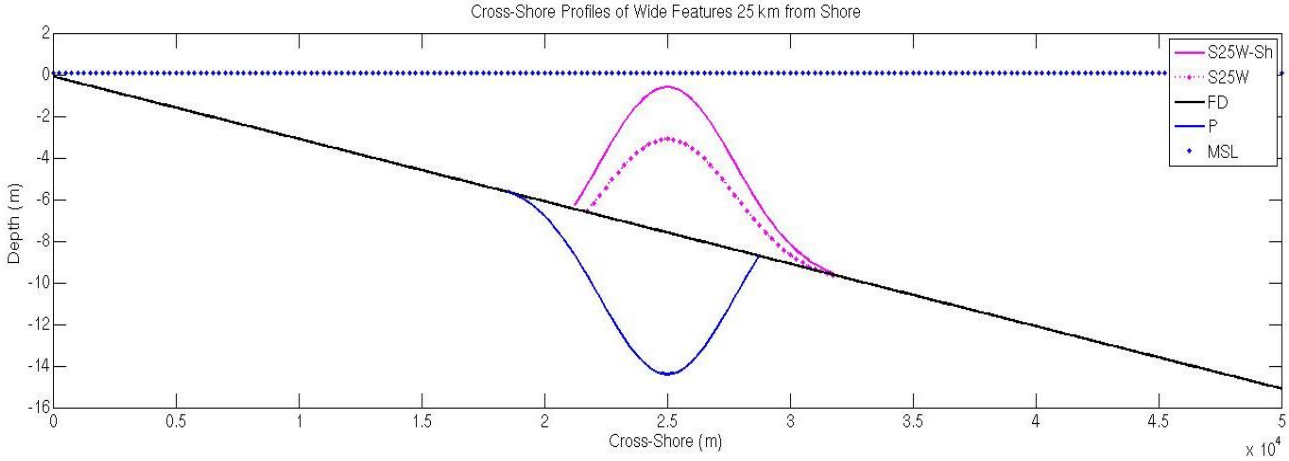

Figure 2-2: Cross-shore profiles of the wide features 25 km from shore. The following domains are depicted from shore to half way down the continental shelf in order to show the various feature elevations relative to mean sea level (MSL): S25W-Sh, with its feature 0.5 m below MSL; S25W, with its feature 3.0 m below MSL; FD to show the elevation at this location in the absence of a feature; and P, with its feature 14.5 m below MSL.

2.2.3. Creation of Local-Scale Bathymetry Features

2.2.3.1. Application of Feature Relief

The process of creating realistic features using idealized geometries is outlined below. In plan-view each bathymetry feature is elliptical in shape. To create a feature's elevation, depths associated with a Gaussian function are applied over the ellipse. The surface formed is symmetric with respect to the major axis of the ellipse, which runs in the alongshore direction.

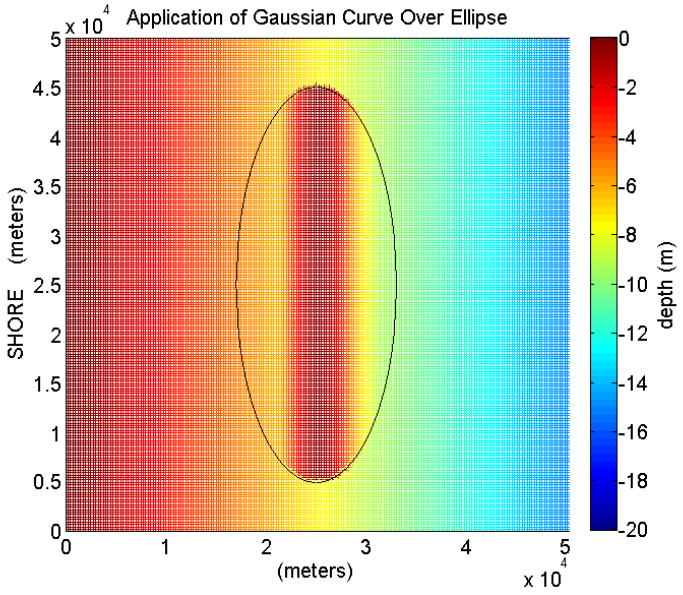

Figure 2-3: Sample sub-domain (plan-view) showing the application of a Gaussian curve over an ellipse, oriented along the major axis, to simulate the relief of a shoal. In this image, cross-shore depth selection has already been performed, but alongshore depth selection has not.

2.2.3.2. Cross-Shore Depth Selection

To accomplish the application of the Gaussian curve's elevations solely over the ellipse, cross-shore depth selection criteria were developed and are illustrated in Figures 2-4 and 2-5. The depth of the continental shelf (in the absence of a feature) and the depth of the Gaussian curve are compared at each point along the x-axis (cross-shore). For shoals (Figure 2-4), from the shore to the offshore side of the feature, the shallower depth is retained as the depth of the seafloor at that location. Beyond the offshore side of the feature, the deeper of the two depths is the one retained, which is the elevation of the continental shelf.

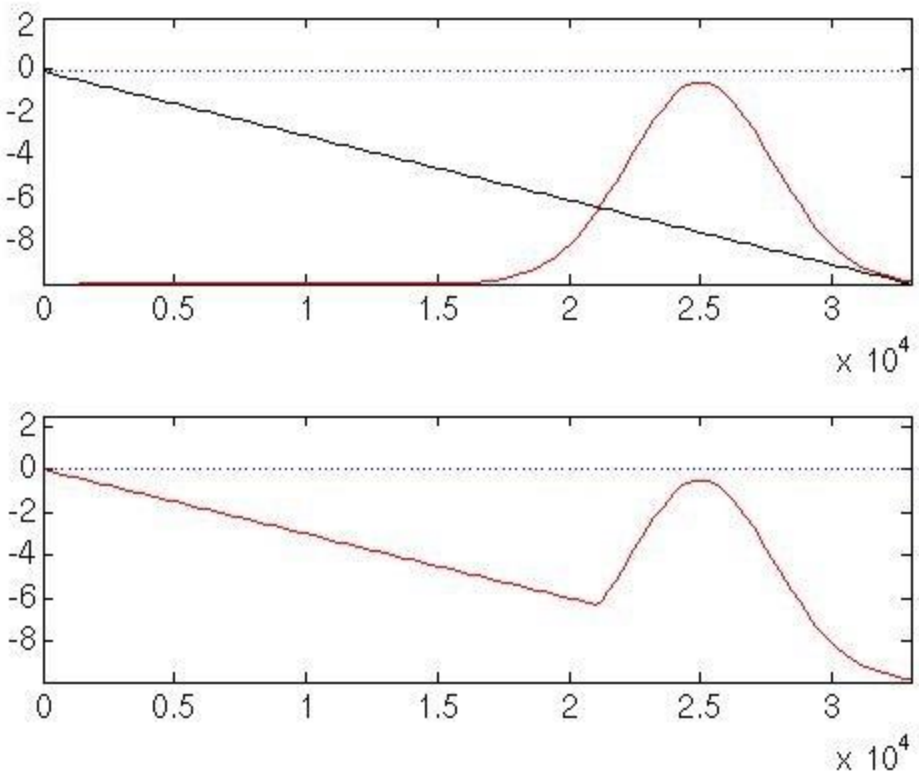

Figure 2-4: Cross-shore depth selection (shoal): (Top) The blue dotted line represents the water's surface. The black line represents the cross-shore profile of the continental shelf in the absence of a feature, and the red curve represents the Gaussian curve used to create the cross-shore profile of the shoal. The depths of the two shapes are compared at each point along the x-axis (cross-shore), and from the shore to the offshore side of the feature, the shallower depth is retained as the depth of the seafloor at that location. Beyond the offshore side of the feature (not pictured), the deeper of the two depths is the one retained, which is the elevation of the continental shelf. (Bottom) The blue dotted line represents the water's surface, and the red curve shows the cross-shore profile after the depth selection process has been completed.

For pits (Figure 2-5), from the shore to the nearshore side of the feature (not pictured), the shallower depth is the one retained, which is the depth of the continental shelf. From the nearshore side of the feature through the most offshore extent of the continental shelf, the deeper elevation is the one retained.

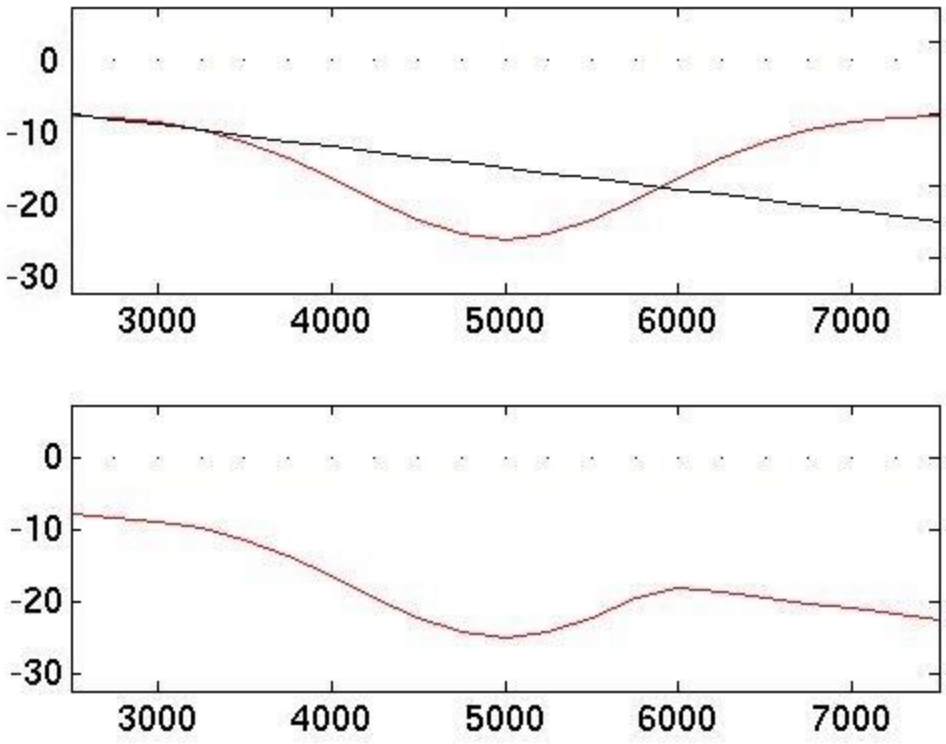

Figure 2-5: Cross-shore depth selection (pit): (Top) The blue dotted line represents the water's surface. The black line represents the cross-shore profile of the continental shelf in the absence of a feature, and the red curve represents the inverted Gaussian curve used to create the cross-shore profile of the pit. The depths of the two shapes are compared at each point along the x-axis (cross-shore), and from the shore to the nearshore side of the feature (not pictured), the shallower depth is the one retained, which is the depth of the continental shelf. From the nearshore side of the feature through the most offshore extent of the continental shelf, the deeper elevation is the one retained. (Bottom) The blue dotted line represents the water's surface, and the red curve shows the cross-shore profile after the depth selection process has been completed.

2.2.3.3. Alongshore Depth Selection

At the ends of the features, depth changes abruptly when going from the Gaussian depths applied over the ellipse to the depths of the surrounding seafloor (Figure 2-6). In order to avoid unrealistic discontinuities in the bathymetry, smoothing of the ends of the features is accomplished by applying a cosine-shaped curve at each end (Figure 2-7). Starting at each narrow end of the ellipse, the depth of each cosine-shaped curve is equal to the depth of the surrounding seafloor at the center of the feature along the major axis of the ellipse. The elevation of each curve increases until, at a distance along the major axis equal to half of the length of the minor axis (half the feature's cross-shore width at its widest point), the curves' elevations are equal to the elevation of the Gaussian curve's peak. The alongshore depth selection process involves comparing the elevation of the cosine-shaped curve and the elevation of the feature at each point along the y-axis (alongshore). For shoals, the deeper of the two elevations is retained at each point of comparison (Figure 2-8). For pits, the shallower elevation is retained at each location.

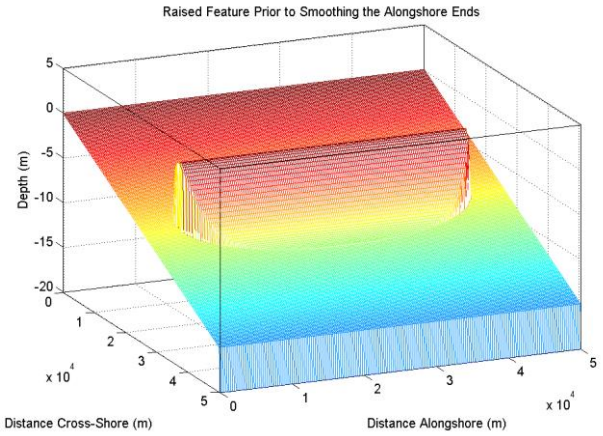

Figure 2-6: Sample sub-domain (same as in Fig. 2-3) showing the application of a Gaussian curve over an ellipse, oriented along the major axis, to simulate the relief of a shoal. In this image, cross-shore depth selection has already been performed, but alongshore depth selection has not.

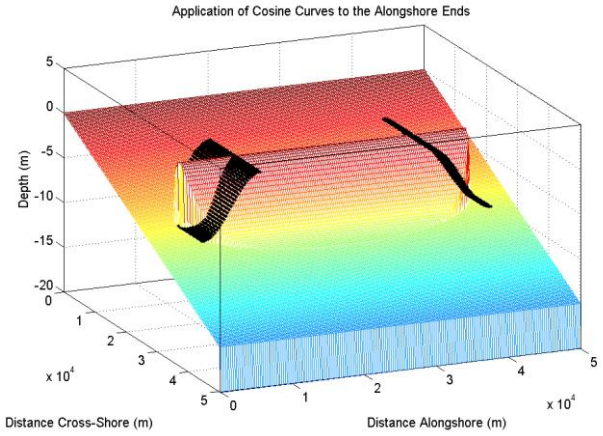

Figure 2-7: Depiction of the cosine-shaped curves (in black) that are part of the alongshore depth selection process used to transition the elevations at the shoal's ends to the elevation of the surrounding seafloor. The alongshore depth selection process involves comparing the elevation of the cosine-shaped curve and the elevation of the feature at each point along the y-axis (alongshore). For shoals, the deeper of the two elevations is retained at each point of comparison.

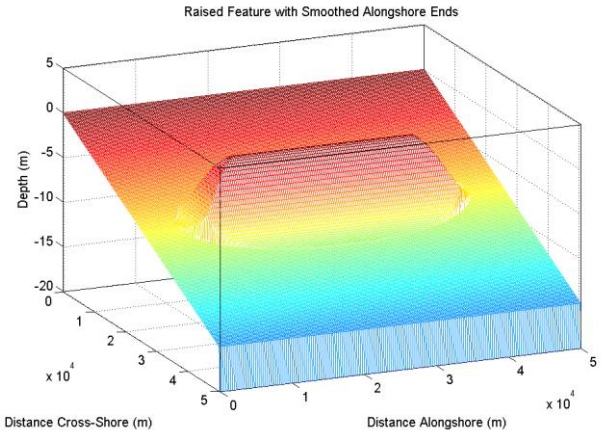

Figure 2-8: Final shape of the shoal after alongshore depth selection has been completed.

2.3. Design of Storms

The tropical cyclones used as forcing for the storm surge model are captured by a simplistic but canonical analytic model by G. J. Holland, Holland (1980). Analytic models arose from the need to recreate storms based on sparse observations. The Holland model is based on the cyclostrophic approximation for wind speed, V_c:

$$V_c = [AB(p_n - p_c)\exp\left(\frac{-A}{r^B}\right)/\rho r^B], \quad (2\text{-}1)$$

where A and B are scaling parameters, p_n is the ambient pressure, p_c is the central pressure, r is the radius, and ρ is the air density (assumed to be constant at 1.15 kg/m^3). The radius to maximum winds is $R_m = A^{1/B}$, so A can be expressed as $R_m{}^B$.

In order to create sea level pressure and wind profiles, the Holland model requires the input of the following parameters (Eq. 2-1): radius of maximum winds (R_m) used to determine A, Holland's B parameter (B), central pressure of the storm (p_c), and environmental (ambient) pressure (p_n). The determination of these parameters will be discussed in detail in Section 2.3.1. Radius of maximum winds is the distance from the center of a tropical cyclone to the location of the cyclone's maximum winds. In well-developed hurricanes, the radius of maximum winds is generally found at the inner edge of the eyewall (Clements, 2009). The shape of the pressure profile is controlled by Holland's B parameter. Holding the radius of maximum winds constant, increasing B causes expansion of the eye and concentrates the pressure drop near the radius of maximum winds, resulting in a steeper gradient. Lower B values cause a more gradual pressure drop beginning near the center of the storm. Larger B values adjust the wind field to give stronger winds near the radius of maximum winds and weaker winds at larger radii (Holland, 1980). Central pressure of the storm and environmental pressure are used to calculate a pressure difference. The value used for environmental pressure is the standard atmospheric pressure of 1013.25 hPa.

Additionally, the storm's track and forward speed are needed by the Holland model in order to generate the time varying wind and pressure fields. The storm's track describes the path that the eye of the storm takes, and forward speed is the translation speed of the storm system (in contrast to rotational speed of the system or maximum velocity, V_m, of the winds). The storm's track and forward speed are incorporated into the Holland model via the longitude and latitude coordinates of the storm's center at 15 minute intervals. All storms used in this study have a uniform forward speed of 6.0 m/s. Three track orientations are used this study: 60, 90, and 120 degrees relative to the landfalling shoreline boundary. (Refer to Figure 1-2 for the definition of track angle.) The spatial resolution of the storm data produced by the hurricane model is 250 m. This value was chosen because 250 m is the highest resolution of the computational mesh used in the surge model.

2.3.1. Determination of Storm Parameters

Two storm sizes were chosen for this study, R_m = 42.4 km and R_m = 60.0 km, in order to assess the sensitivity of the bathymetry features' role in surge generation to storms of varying sizes and intensities. Since the area of a storm is proportional to the square of its radius, the storms with 60.0 km R_m are twice the size of the storms with R_m = 42.4 km. Compact storms are

generally more intense than larger storms so, typically, as R_m decreases, storm intensity increases. Given that storm size was prescribed, realistic values for other required parameters were calculated using the following relationships.

2.3.1.1. Calculation of Maximum Wind Speed

The maximum wind speed, V_m, for each size storm was found using Eq. 2 from Gross et al. (2004). The latitude, θ, chosen is 30° N because locations at this latitude are commonly affected by tropical cyclones, and it is appropriate to the Northern Gulf of Mexico.

$$R_m = 35.37 - 0.111V_m + 0.570(\theta - 25), \tag{2-2}$$

where R_m = radius of maximum winds (nmi)
V_m = maximum wind (kt)
θ = latitude (ºN)

2.3.1.2. Calculation of Central Pressure

Knaff and Zehr (2007) fit a wind-pressure relationship (WPR) based on gradient wind balance to the dataset used by Atkinson and Holliday (1975) that Knaff and Zehr binned by storm intensity. Given the maximum wind speed, V_m, and a reference pressure, P_{ref}, the central pressure is obtained from a table provided by Knaff and Zehr (2007) that is based on the equation:

$$\Delta p = 11.48 - 0.73V_m - \left(\frac{V_m}{107.21}\right)^2, \tag{2-3}$$

where $\Delta p = P_{ref} - p_c$
p_c = central pressure (hPa)
P_{ref} = 1010 (hPa), the value for P_{env} used by Knaff and Zehr (2007)
V_m = maximum wind (kt)

2.3.1.3. Calculation of Holland's B Parameter

Using the values for the storm's central pressure, p_c, environmental pressure, p_n, and the radius of maximum winds, R_m, Holland's B parameter can be calculated using Eq. 5 from Vickery and Wadhera (2008):

$$B = 1.38 - 0.00184\Delta p + 0.00309R_m, \tag{2-4}$$

where B = Holland's B parameter
Δp = the difference between the environmental pressure p_n and central pressure p_c (hPa)
R_m = radius of maximum winds (km)

2.3.2. Storm Parameters Used in this Study

The values of the parameters used in creating each storm can be found in Table 2-2. The maximum wind speeds of the storms with a R_m of 60.0 km correspond to a tropical storm (Webster et al., 2005). The storms with a R_m of 42.4 km have maximum wind speeds and central pressure corresponding to a Category 5 hurricane on the Simpson and Saffir (1974) scale.

Table 2-2: Parameters of the two storms used in this study. The smaller, more powerful storm's parameters are in pink, and the larger, more diffuse storm's parameters are in lavender.

Storm Parameters				
Radius to Maximum Winds (km)	Holland's B Parameter	Central Pressure (hPa)	Maximum Wind Speed (m/s)	Forward Speed (m/s)
42.4	1.34	919	71.0	6.0
60.0	1.51	983	27.0	6.0

2.4. Surge Model Description

The ADvanced CIRCulation (ADCIRC) model is a highly developed computer program for solving the equations of motion for a moving fluid on a rotating earth (Luettich et al., 1992). ADCIRC was developed to provide a more accurate technique for predicting sea surface elevation and currents in coastal areas. It is used for computing features of circulation patterns driven by tides, wind, and atmospheric pressure gradients (Luettich et al., 1992), and it is widely used for modeling storm surge (Blain et al., 1994; Irish et al., 2008; Rego and Li, 2009; Weaver and Slinn, 2010; and Li et al., 2013) and coastal inundation (Rego and Li, 2009). ADCIRC utilizes highly flexible unstructured grids based on finite elements. This allows for excellent characterization of complex geometries with the ability to have high resolution in areas of interest and lower resolution away from those areas. Therefore, one can have a large domain allowing for the use of open water boundary conditions without having to include large quantities of information to characterize areas far from the region of interest (Luettich et al., 1992).

2.4.1. Simplifying Assumptions (Shallow Water Formulation)

ADCIRC is designed to model long-wave circulation by applying the Reynolds-averaged, Navier-Stokes equations, simplified using the Boussinesq and the hydrostatic pressure approximations. As a result, ADCIRC's solutions are valid for nearly horizontal flow. Inherent in this formulation are the following assumptions (Kinnmark, 1985):

1. Reynolds-averaging – An approximate time-averaged solution for velocity can be obtained through separating flow into mean and fluctuating quantities and treating the fluctuating part of the solution (turbulence) using vertical turbulent closure.

2. Boussinesq approximation – Density fluctuations are small, and in terms where density is not multiplied by gravitational acceleration, the variation in density can be replaced by a constant value for density.

3. Hydrostatic approximation – Vertical accelerations are small compared to the acceleration of gravity (the horizontal scale is far greater than the vertical scale so that there is negligible variation in density over the depth) so that the vertical pressure gradient may be given as the product of density, gravity, and depth.

ADCIRC Two-Dimensional Depth-Integrated (2DDI) solves the Generalized Wave Continuity Equation (*GWCE*) (Equation 2-5), which is a linear combination of the depth-integrated primitive continuity equation (*PCE*) (Equation 2-6) and the depth-integrated momentum equation (*M*) (Equation 2-7).

$$\frac{\partial(PCE)}{\partial t} + \tau_0(PCE) - \nabla \cdot M = 0 \qquad (2\text{-}5)$$

τ_0 is the *GWCE* weighting parameter used to optimize numerical accuracy, where $\tau_0 \rightarrow \infty$ results in a pure wave equation and $\tau_0 \rightarrow 0$ results in a pure continuity equation. The *GWCE* formulation prevents the generation of non-physical solutions that can arise from finite element (FE) discretization of the *PCE*. It also allows for time-independent system matrices which require less computational resources than time-dependent matrices that must be assembled and solved at every time step. The *GWCE* formulation is applied prior to any numerical discretization (Kinnmark, 1985).

$$\frac{\partial \zeta}{\partial t} + \frac{\partial UH}{\partial x} + \frac{\partial VH}{\partial y} = 0, \qquad (2\text{-}6)$$

where ζ = free surface elevation relative to the geoid
$H = \zeta + h$ is the total water depth to the free surface, where h = bathymetric depth relative to the geoid
U = zonal depth-averaged horizontal velocity
V = meridional depth-averaged velocity

$$\frac{\partial \mathbf{v}}{\partial t} + \mathbf{v}\nabla \cdot (\mathbf{v}) + \mathbf{f} \times \mathbf{v} + \nabla\left[\frac{p_a}{\rho_0} + g(\zeta - \alpha\eta)\right] - \frac{\boldsymbol{\tau}_s + \boldsymbol{\tau}_b}{\rho_0 H} - \frac{\boldsymbol{\varepsilon}}{H}\nabla^2(H\mathbf{v}) = 0 \qquad (2\text{-}7)$$

For the momentum equation (Equation 2-7), the physical meanings of the terms are described in Figure 2-9.

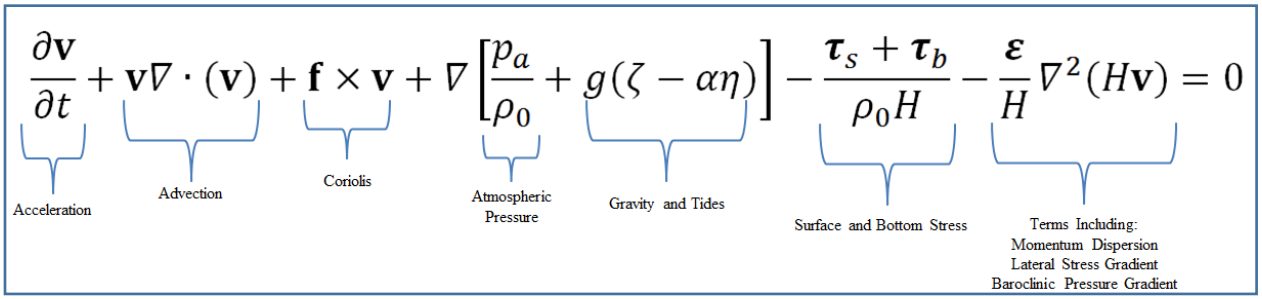

Figure 2-9: The momentum equation with a description of the physical meaning of each term.

2.4.2. Temporal Discretization

The equations are first discretized in time using the finite difference (FD) method. In the FD method, derivatives in an equation are replaced with Taylor-series approximations of those derivatives which can be solved algebraically. ADCIRC utilizes an explicit time-stepping method. In an explicit FD method, the solution at a particular time step is dependent only on the

solution at the previous time step. Explicit methods are computationally inexpensive to implement, but they can suffer from instabilities if the Courant–Friedrichs–Lewy (CFL) condition is not met. This criterion is a ratio of the time step to the spatial interval (or some power of the spatial interval based on the order of the differential equation being approximated) and thus restricts how large a time step can be used in order to not have, e.g., a wave travel a greater distance than the highest mesh resolution in one time step, resulting in inaccuracies (Courant et al., 1967). ADCIRC uses different temporal discretization for the continuity and momentum equations. For the continuity equation, the time derivatives are discretized over three levels, so that the solution for the future water level requires knowledge of the present and past water levels. For the momentum equation, the temporal discretization is explicit for all terms except Coriolis, which uses an average of the present and future velocities (Luettich et al., 1992).

2.4.3. Spatial Discretization

Finite element (FE) discretization is applied to the time-discretized form of the governing equations to complete their conversion into systems of algebraic equations suitable for numerical solution. The FE method is a numerical technique used to approximate the solution to a boundary-value problem, which is a differential equation together with a set of boundary conditions. The FE technique uses variational methods to minimize an error function and produce a stable solution. ADCIRC uses a continuous Galerkin FE method. The FE method provides maximum grid flexibility and allows highly efficient numerical solutions to be obtained using model domains that include complicated bathymetries and shoreline geometries that also stretch considerable distances offshore to implement open-water boundary conditions (Luettich et al., 1992). FE algorithms based on triangular elements are highly flexible and can provide local grid refinement in a systematic and optimal fashion (Luettich et al., 1992). The ability to vary resolution over the domain (grid flexibility) is pivotal to solution accuracy and computational efficiency. Accuracy is improved by having high resolution near shore and in areas where flow and/or geometry vary rapidly. The ability to have lower resolution away from areas of high variation reduces the computational resource requirement.

2.4.3.1. Construction of Computational Mesh

Creation of the computational meshes was accomplished using xmGredit5 (Turner, 1999) and MeshGUI (Blain et al., 2008). The finite element mesh of each domain, consisting of triangular elements, had 4,000 m resolution over the abyssal plain. Four depth-based refinements were made at depths of 1,990 m, 1,340 m, 690 m, and 40 m, resulting in 250 m resolution just before reaching the continental shelf break, and continuing to shore. The featureless reference domain had 796,743 nodes and 1,590,625 elements.

2.4.4. Implementation of Surge Model

Simulations are performed using ADCIRC v50.99.05 in barotropic, two-dimensional depth-integrated mode (2DDI). Two boundary types are used, an elevation boundary at the open water edges of the domain and a mainland boundary at the shore. Elevation, η, was specified at each node of the open water boundary. It was chosen to be constant and equal to MSL (η = 0.0000). The shore boundary allowed no normal flow but had no constraint on tangential flow, as it was representative of a mainland boundary. Wind stress and atmospheric pressure were input to all grid nodes every 15 minutes (900 s), which is not equal to the model time step (1 s), so interpolation in time was used to synchronize the wind and pressure information with the model

time step. Wetting and drying of elements was enabled, and the depth for a node and surrounding elements to be considered dry was 0.01 m. A dry node wets if a water surface slope exists that would drive water from a currently wet node to the dry node and the steady-state current velocity that results would have a velocity > 0.01 ms^{-1}. Initial water depths were assumed equal to the bathymetric water depth specified in the grid file. A hybrid nonlinear bottom friction formulation was used (Equation 2-8).

$$C_D = max\left\{C_{D\,min}\left(1+\left(\frac{H_{break}}{H}\right)^{\theta}\right)^{\frac{\gamma}{\theta}}, 10^{-4}\right\}, \tag{2-8}$$

where $C_{D\,min}$ is either a linear or quadratic drag coefficient, H is the total water column depth, and H_{break} is the depth at which waves break. According to Luettich and Westerink (1995), the exponent θ determines how rapidly C_D approaches each asymptotic limit, while the exponent γ controls the rate at which the friction coefficient increases as the water depth increases (Blain et al., 2010). In deep water, the friction coefficient is constant and a quadratic bottom friction law results; whereas in shallow water (less than 1.0 m), the friction coefficient increases as the depth decreases. The minimum value of the friction coefficient, 0.0025, is approached in deep water where the hybrid friction relationship reverts to a quadratic function of depth-averaged velocity. A spatially variable Coriolis parameter was computed based on latitude. Advective terms were not included in the computations. A hyperbolic tangent ramp function was specified and applied to forcing. Since these simulations had only meteorological forcing (i.e. wind and atmospheric pressure), a 1-hour ramp (3600 time steps) was sufficient. During the ramp, the storm forcings were held stationary. After the completion of the ramp, the wind and pressure fields vary in time, representing the storm's translation through the domain.

2.5. Methods of Analysis

2.5.1. Selection of Recording Station for Elevation Analysis

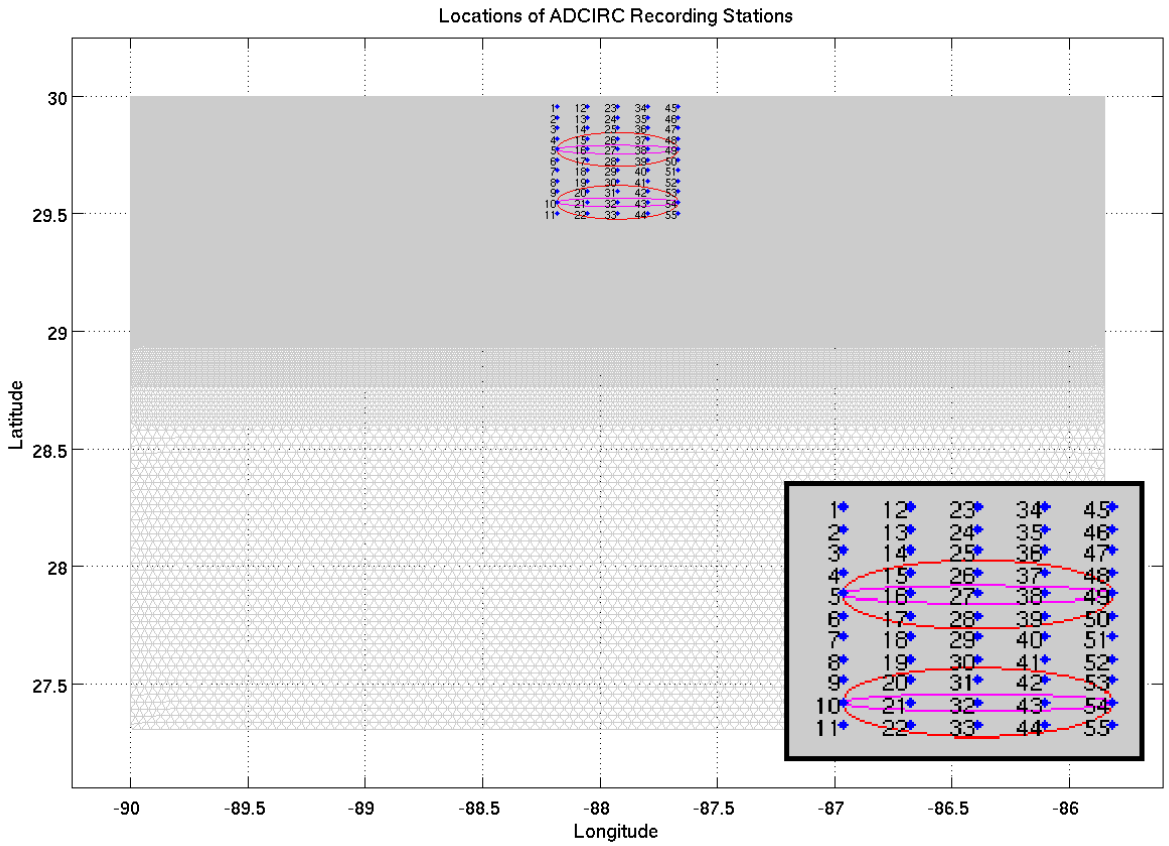

Figure 2-10: Locations of recording stations in each domain. Elevation and velocity were recorded at 15 minute intervals throughout the simulations at these locations (global elevation and velocity were recorded hourly). An enlarged view of the stations, shown with respect to the features' locations, is shown in the lower right corner of the figure.

Recording Station 36, located 15 km from shore and 12.5 km to the east of the center of the domains, was chosen as the location where surge response to the features was thoroughly examined. Its distance from shore, 15 km, was chosen as to avoid any unrealistic surge that results from proximity to the shoreline boundary, yet it is shoreward of all features so that the storms will have interacted with the features by the time surge arrives at the station. Its position 12.5 km east of the center of the domain locates it within the northeast quadrant of each storm. Output at other stations was examined prior to selecting Station 36. The system (domains and storms) is fairly symmetric, but this location had some advantages. It is a location at which setup occurs on the nearshore side of the shoals during surge recession (at least on the shoals 25 km from shore), which leads to a good characterization of the shoals' total influence.

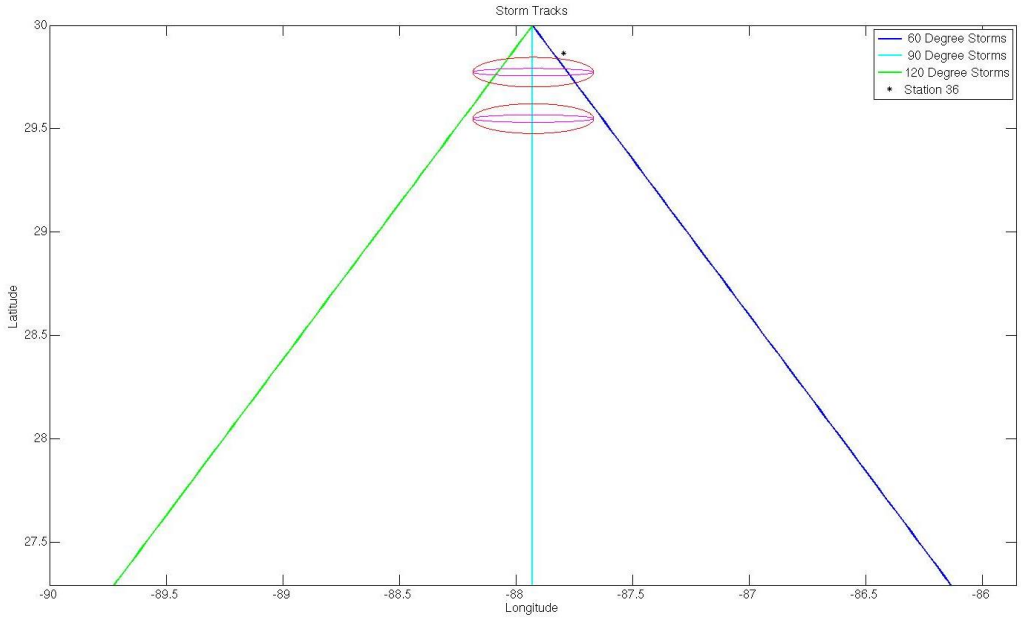

Figure 2-11: Image of the entire domain showing the location of Recording Station 36 relative to the features and the storm tracks. Station 36 is in a location where the northeast quadrant of each storm passes over. Though the tracks appear to end at the shore (top of the image), the storms progress inland beyond the shoreline allowing the storm conditions over water to gradually diminish.

After completion of the simulations, elevations at Recording Station 36 in all ten domains were compared for each storm, looking for differences in elevation between the domains. Times at which to examine the surge response were chosen based on the occurrence of elevation differences, indicating feature influence on surge response at that time. Even though there was not a noticeable difference in elevation in the various domains at the time of maximum elevation, peak surge was still considered to be of interest. The other times at which surge response to the features was examined were three hours after landfall for all storms and four and a half hours before landfall during a particular storm in which there was a large difference in elevation from one domain to the next.

Once the times at which the features influenced surge were determined, the following techniques were employed to determine which feature characteristics were most influential to surge generation and how the surge response varied under different storm conditions.

2.5.2. Calculation of Each Feature's Influence on Surge Generation

At each time of interest (i.e. peak surge, three hours after landfall, and during the pre-landfall set-down that occurred during one storm), the difference in elevation (cm) between domains with features and the featureless reference domain (FD) was calculated:

$$Elevation\ Difference\ (cm) = (\eta_i - \eta_0) \times 100,\ i \neq 0, \qquad (2\text{-}9)$$

where η_0 is the elevation in the featureless reference domain (FD), and η_i represents elevation in a domain with a feature.

Secondly, elevations in domains with features were compared with the elevation in the FD to determine percent change in elevation from the FD:

$$\%\ Change\ from\ FD = \frac{\eta_i - \eta_0}{|\eta_0|} \times 100\ ,\ i \neq 0, \tag{2-10}$$

where η_0 is the elevation in the featureless reference domain (FD), and η_i represents elevation in a domain with a feature.

Elevation difference in centimeters from the FD and percent change from the FD were the primary metrics used in determining a feature's influence on surge generation.

2.5.3. Determination of Feature Influence on Surge Generation by Feature Class

Feature classes were defined to determine which bathymetry feature characteristics were the most influential to surge generation. In order to understand how a particular parameter, e.g., depth below MSL, influenced surge generation, the eight shoals were divided into two groups. The first group's shoals had one value of the parameter being examined, e.g., a depth of 0.5 m below MSL, and the second group's shoals had the alternative value of that parameter, a depth of 3.0 m below MSL. Each group is what will be referred to as a feature class. In this example, the shoals that were 0.5 m below MSL make up the class of shallow features (Table 2-3; A. shoals in gold ending with -Sh), and the shoals that were 3.0 m below MSL comprise the class of deep features (Table 2-3; A. shoals in lavender). Since three parameters (i.e., depth below MSL, cross-shore width, and distance from shore) were examined, division of the eight shoals according to alternative values of each parameter results in six feature classes (Table 2-3; A-C). Table 2-3; B. shows division of the shoals according to alternative values of cross-shore width. The wide features are in peach, and their names contain the letter W. The narrow features are in blue. Table 2-3; C. shows division of the shoals according to alternative values of distance from shore. The close features are in green, and they have 25 in their names, indicating that they are 25 km from shore. The distant features are in white, and they have 50 in their names, indicating that they are 50 km from shore.

Table 2-3 (A-C): Division of the eight shoals into six parameter-based feature classes: A. (Left) Division by shoal depth below MSL with shallow features in gold and deep features in lavender; B. (Center) Division by shoal cross-shore width with wide features in peach and narrow features in blue; C. (Right) Division by shoal distance from shore with close features in green and distant features in white.

A. Comparison by Depth below MSL	
S50	S25
S50W	S25W
S50-Sh	S25-Sh
S50W-Sh	S25W-Sh

B. Comparison by Cross-Shore Width	
S50	S25
S50W	S25W
S50-Sh	S25-Sh
S50W-Sh	S25W-Sh

C. Comparison by Distance from Shore	
S50	S25
S50W	S25W
S50-Sh	S25-Sh
S50W-Sh	S25W-Sh

After these classes were constructed, the mean elevation difference from the FD was calculated for each class and ranked from greatest to least to determine which feature classes

(e.g., wide features, shallow features, etc.) were most influential on surge generation. The comparison of class influence need not be limited to within each parameter because regardless of which parameter the shoals were grouped by (according to alternative values of that parameter), the total elevation difference from the FD (the sum over all eight domains) was a fixed value. For each comparison (A., B., and C. in Table 2-3), each pair of classes had different proportions of the total elevation difference from the FD. Ranking each class' mean elevation difference from the FD allowed for the determination of the relative influence of each class on surge generation at the time of comparison.

This division into classes also allowed for a way to determine the sensitivity of surge generation to the three parameters considered. Within a given parameter (e.g., depth below MSL), the larger the difference between each class's mean elevation difference from the FD (i.e., that of the shallow features and of the deep features), the more sensitive surge generation is to that parameter. If the mean elevation difference from the FD is similar for classes with alternative values of a given parameter, that implies that surge generation is relatively insensitive to that parameter. The evaluation of surge response by feature class was done at three hours after landfall for all storms and during the setdown that occurred four and a half hours before landfall during one storm.

2.5.4. Evaluation of Sensitivity of Surge Response to Storm Conditions

In one instance, three hours after landfall, surge response to feature class was evaluated for all storms. This provided an opportunity to examine the sensitivity of surge response to storm conditions. A mean surge response by feature class was calculated, which included the surge response to all storms, but in order to examine the influence of the storm conditions, surge response was also evaluated by storm size/intensity and by storm track. Table 2-4; A. shows the groupings for evaluation of surge response by storm size. The smaller, more intense storms are colored peach, and the larger, less intense storms are colored blue. Table 2-4; B. shows the grouping for evaluation of surge response by storm track. The storms that approached from the Southeast (60° track) are colored green, the storms with a shore-normal approach (90° track) are colored white, and the storms that approached from the Southwest (120° track) are colored lavender. Finally, surge response to each individual storm was analyzed.

Table 2-4 (A-B): Storms grouped by parameter: A. (Left) Storms grouped by size. The smaller, more intense storms with a R_m of 42.4 km are colored peach, and the larger, less intense storms with at R_m of 60.0 km are colored blue; B. (Right) Storms grouped by track. The storms that approached from the Southeast (60° track) are colored green, the storms with a shore-normal approach (90° track) are colored white, and the storms that approached from the Southwest (120° track) are colored lavender.

A. Comparison by Storm Size	
42.4 km 60°	60.0 km 60°
42.4 km 90°	60.0 km 90°
42.4 km 120°	60.0 km 120°

B. Comparison by Storm Track	
42.4 km 60°	60.0 km 60°
42.4 km 90°	60.0 km 90°
42.4 km 120°	60.0 km 120°

2.5.5. Spatial Analyses to Determine Causes of Observed Surge Response

Analyses of the spatial variability of global conditions such as elevation, wind stress, and water velocity were used to assist in determining the causes of the observed surge response when analyzing the elevation time series at Recording Station 36. The following plots were created for this purpose:

i. Plots of surface elevation (shown using colored contour lines) and water velocity (magnitude and direction shown using arrows). When the plots were of domains with a feature, the outline of the feature was depicted in order to show the elevation and water velocity in reference to the feature. The location of Recording Station 36 in each plot was shown using a red asterisk.

ii. Wind stress plots that used color to show the magnitude of the wind stress and vectors showing both magnitude and direction. The outlines of the largest features located each distance from shore were plotted to show the direction of the winds with respect to the features. Additionally, the storm track was plotted to help the viewer understand the pictured storm's trajectory. The location of Recording Station 36 was shown using a red asterisk.

The spatial analyses were used to assess the development of surge conditions over time or through the comparison of concurrent snapshots of different systems to better understand the role of feature or storm differences.

3. Results and Discussion

3.1. Overview of Results

The features considered in this study were locally influential to surge generation but only at certain times during the passage of the storms through the domains. This is indicated by the fact that the differences in elevation amongst the various domains, visible in the elevation time series plots from Recording Station 36 (Figures 3-1, 3-2, and 3-3), only exist at certain times, and at other times the elevations are nearly identical. At the time of peak surge, elevations were not meaningfully influenced by the presence of bathymetry features, but in some cases the same features delayed the arrival of peak surge at Recording Station 36. Surge response at Station 36 was examined at two other times: 3 hours after all storms made landfall during the recession of surge and 4.5 hours before landfall of the smaller (42.4 km R_m) storm approaching from the southeast (60° track) when there was setdown due to the direction of the winds. During those two times when the surge response was examined, the presence of the features was noticeably influential on surge generation. (These times are indicated by gold vertical lines in Figures 3-1, 3-2, and 3-3). At those times, surge response was examined by feature class, and in all cases, the shallow shoals were the most influential on surge generation, and the deep ones had the least impact. The order of influence of the other feature classes on surge generation varied according to the storm conditions.

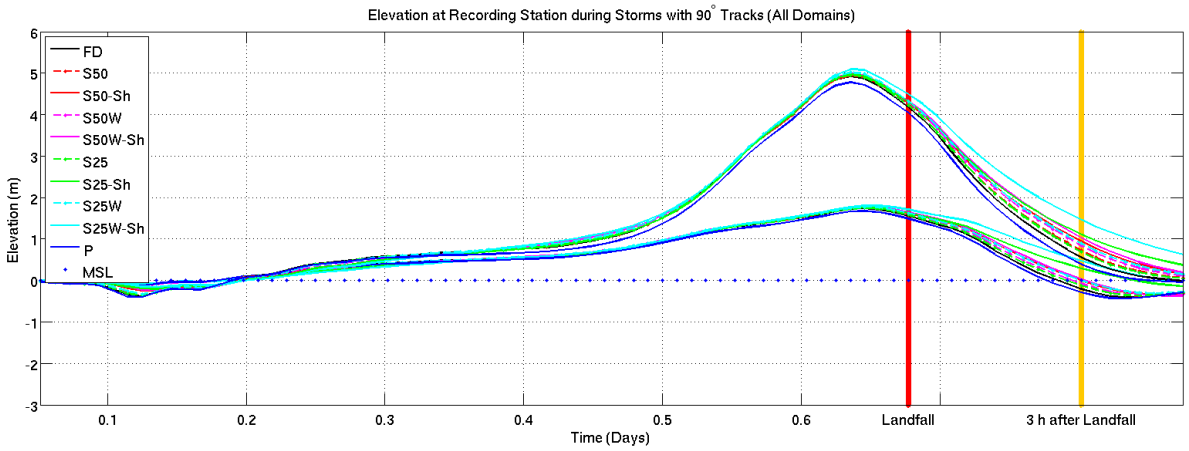

Figure 3-1: Elevation in all domains at Recording Station 36 during storms with shore-normal (90°) tracks. The upper curve shows water levels during the storm with R_m = 42.4 km. The lower curve shows water levels during the storm with R_m = 60.0 km. Time of landfall is indicated by the red vertical line, and three hours after landfall is indicated by the gold vertical line.

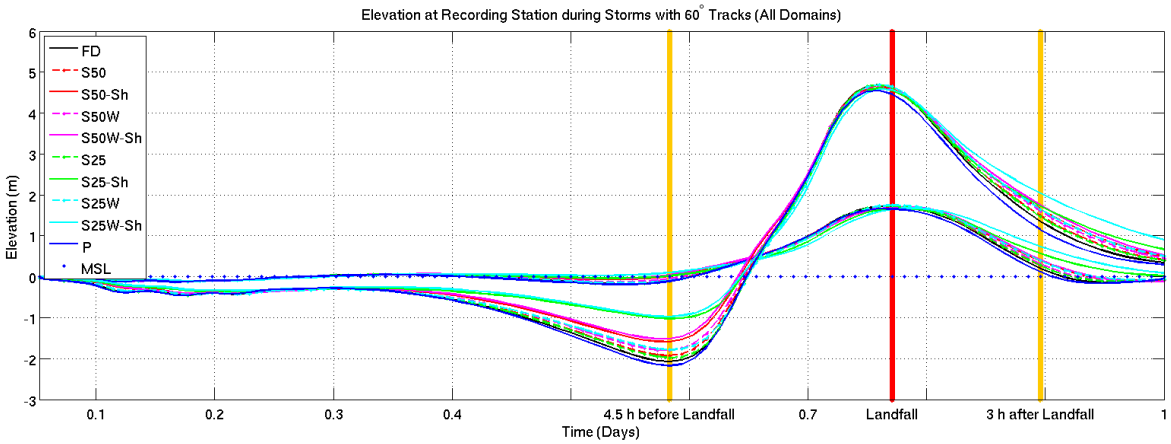

Figure 3-2: Elevation in all domains at Recording Station 36 during storms with 60° tracks (approach from the southeast). The curve with the highest peak shows water levels during the storm with R_m = 42.4 km. The flatter curve shows water levels during the storm with R_m = 60.0 km. The time of the pre-landfall elevation minimum caused by setdown during the smaller storm is indicated by the gold vertical line on the left. Time of landfall is indicated by the red vertical line, and three hours after landfall is indicated by the gold vertical line on the right.

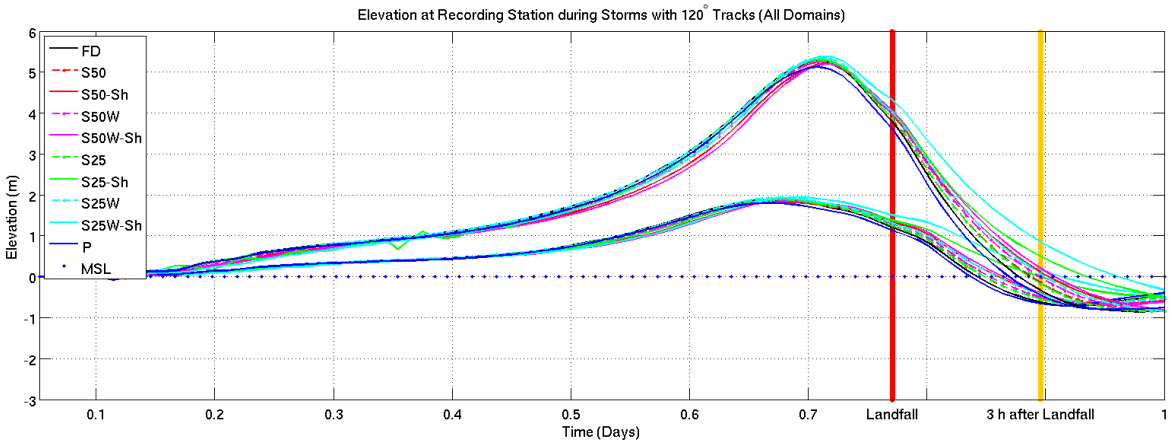

Figure 3-3: Elevation in all domains at Recording Station 36 during storms with 120° tracks (approach from the southwest). The upper curve shows water levels during the storm with R_m = 42.4 km. The lower curve shows water levels during the storm with R_m = 60.0 km. Time of landfall is indicated by the red vertical line, and three hours after landfall is indicated by the gold vertical line.

3.2. Examination of Peak Storm Surge

3.2.1. Characteristics of Peak Surge Subject to Differing Storm Conditions

As expected, the smaller, more intense storms caused greater peak elevations (Table 3-1, right, gold) than the larger, less intense storms (Table 3-1, left, pale gold). For storms with a R_m of 42.4 km, the average peak elevation at Recording Station 36 was 4.95 m above MSL, and it was 1.78 m above MSL for storms with a R_m of 60.0 km (calculated using values in Table 3-1).

Table 3-1: Maximum elevation (meters) in each domain during each storm at Recording Station 36, colors indicating increase in elevation with decreasing storm size. The larger (R_m = 60.0 km), more diffuse storms produced lower peak elevations (left, pale gold). The smaller (R_m = 42.4 km), more intense storms produced higher peak elevations (right, gold).

Peak Surge (m)						
Domain	60.0 km 60° Track	60.0 km 90° Track	60.0 km 120° Track	42.4 km 60° Track	42.4 km 90° Track	42.4 km 120° Track
FD	1.7209	1.7344	1.8835	4.6833	4.9221	5.2725
S50	1.7243	1.7537	1.8681	4.6719	4.9439	5.2561
S50W	1.7285	1.7861	1.8756	4.6579	4.9899	5.2617
S50-Sh	1.6912	1.7663	1.8284	4.6148	4.9409	5.1934
S50W-Sh	1.7014	1.7939	1.8404	4.5858	4.9800	5.1995
S25	1.7296	1.7477	1.8957	4.6864	4.9519	5.2973
S25W	1.7460	1.7753	1.9293	4.6976	5.0178	5.3525
S25-Sh	1.6703	1.7602	1.8888	4.6067	4.9742	5.3102
S25W-Sh	1.6691	1.8064	1.9388	4.5809	5.0892	5.3849
P	1.6597	1.6740	1.8053	4.5405	4.7742	5.1313

For each storm size, peak elevation increased with increasing track angle for the three tracks considered (60°, 90°, and 120°) (Table 3-2). The following percent change values were calculated using elevations from Table 3-2. For the larger (R_m = 60.0 km), less intense storms, the storm approaching from the southwest (120° track) caused a mean increase in peak elevation of 6.57% compared with the shore-normal approach, and the storm approaching from the southeast (60° track) caused a mean decrease in peak elevation of 3.17%. For the smaller (R_m = 42.4 km), more intense storms, the storm approaching from the southwest caused a similar mean increase in peak elevation (6.20%) from the shore-normal approach as the larger storm. However, the smaller storm approaching from the southeast caused a larger decrease in peak elevation (6.57%) than the large storm approaching from the southeast. It is likely that the substantial setdown that occurred prior to the arrival of peak surge during the smaller, more powerful storm contributed to the decreased peak surge level. The impact of landfall direction on peak elevation found in this study (an increase in peak surge for track angles greater than 90° and a decrease in peak surge for track angles less than 90°) is consistent with the findings of Irish et al. (2008) who found that all storm tracks with more westerly headings (45°-75°) produced smaller surges than the due north (90°) track for both moderately and mildly sloping bottoms. For the most mildly sloping bottom (1:10,000), storms with more easterly headings (105°-150°)

produced surges that were as large, or slightly larger (no more than 8%), than the due north (90°) track.

Table 3-2: Maximum elevation (meters) in each domain during each storm at Recording Station 36, colors indicating increase in elevation with increasing storm track angle. For each size storm, peak elevations increased with increasing track angle. Storms with 60° tracks (approach from the southeast) caused the lowest peak elevations (pale gold). Storms with 90° tracks (shore-normal approach) caused greater peak elevations than the 60° tracks (gold), and storms with 120° tracks (approach from the southwest) caused the highest peak elevations of the three tracks considered (deep gold). (Note that these are the same elevations shown in Table 3-1.)

Simulations Performed						
Domain	60.0 km 60° Track	60.0 km 90° Track	60.0 km 120° Track	42.4 km 60° Track	42.4 km 90° Track	42.4 km 120° Track
FD	1.7209	1.7344	1.8835	4.6833	4.9221	5.2725
S50	1.7243	1.7537	1.8681	4.6719	4.9439	5.2561
S50W	1.7285	1.7861	1.8756	4.6579	4.9899	5.2617
S50-Sh	1.6912	1.7663	1.8284	4.6148	4.9409	5.1934
S50W-Sh	1.7014	1.7939	1.8404	4.5858	4.9800	5.1995
S25	1.7296	1.7477	1.8957	4.6864	4.9519	5.2973
S25W	1.7460	1.7753	1.9293	4.6976	5.0178	5.3525
S25-Sh	1.6703	1.7602	1.8888	4.6067	4.9742	5.3102
S25W-Sh	1.6691	1.8064	1.9388	4.5809	5.0892	5.3849
P	1.6597	1.6740	1.8053	4.5405	4.7742	5.1313

3.2.2. Effect of Bathymetry Features on Peak Storm Surge

3.2.2.1. Overview of Impact of Features on Peak Surge

The presence of the bathymetry features considered in this study had negligible impact on peak storm surge levels. This was made evident by the fact that for any given storm, the peak elevations at Recording Station 36 in domains with features were nearly the same as in the featureless reference domain (FD) (Tables 3-1 and 3-2). An effect that some of the features did have on peak surge was that their presence caused a small delay in its arrival during the storms that did not have a shore-normal approach. Peak elevation during the shore-normal storms is shown in Figure 3-4. In the inset it is visible that during the smaller storm the domain with the pit (P) had decreased elevation compared with the reference domain (FD) of ≈ 15 cm and that the domain with the close, wide, shallow shoal (S25W-Sh) had increased elevation of a similar magnitude. Considering that the peak elevation in the FD was ≈ 5 m, this was only a change of ≈ ±3%. During the storms approaching from the southeast, there was a small delay in the arrival of peak surge in the domains with close, shallow shoals. The delay during the smaller storm is visible in the inset of Figure 3-5. The delay in the arrival of peak surge in these domains was actually more prominent during the larger (R_m = 60.0 km) storm in which water levels were lower. During the small storm approaching from the southwest, there was a small delay in the arrival of peak surge in the domains with distant, shallow shoals. This is visible in the inset of Figure 3-6.

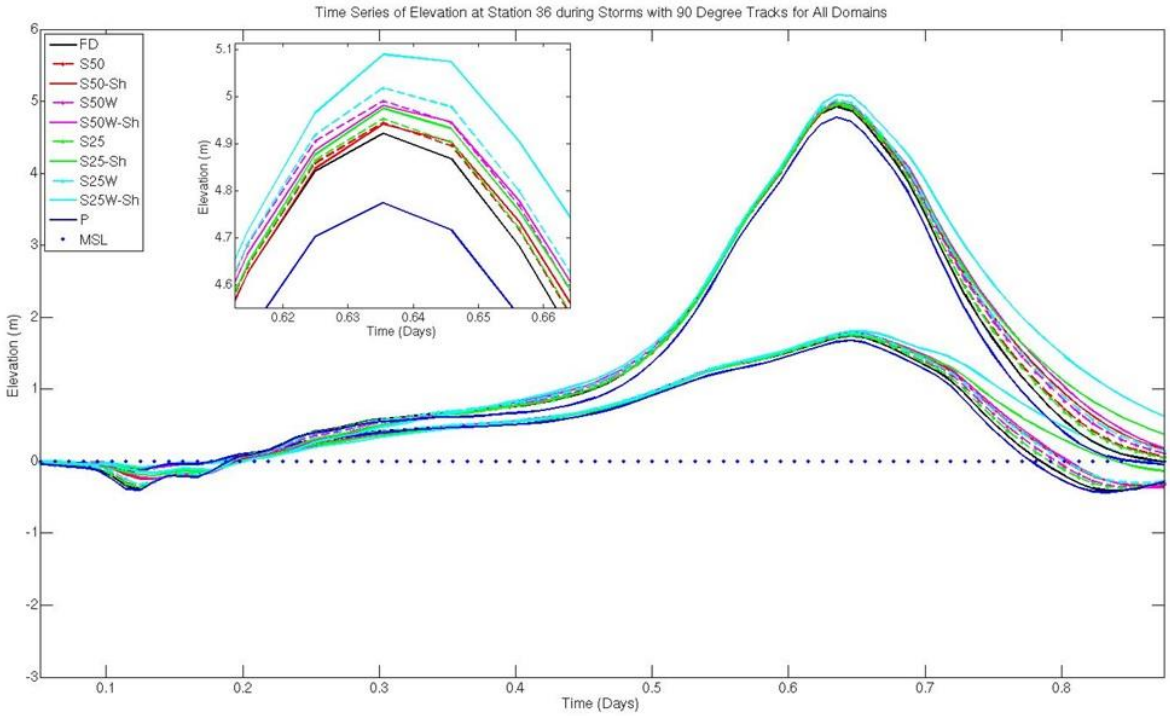

Figure 3-4: Elevation in all domains at Recording Station 36 during storms with 90° tracks, with inset showing peak elevation in each domain during the smaller (R_m = 42.4 km) storm.

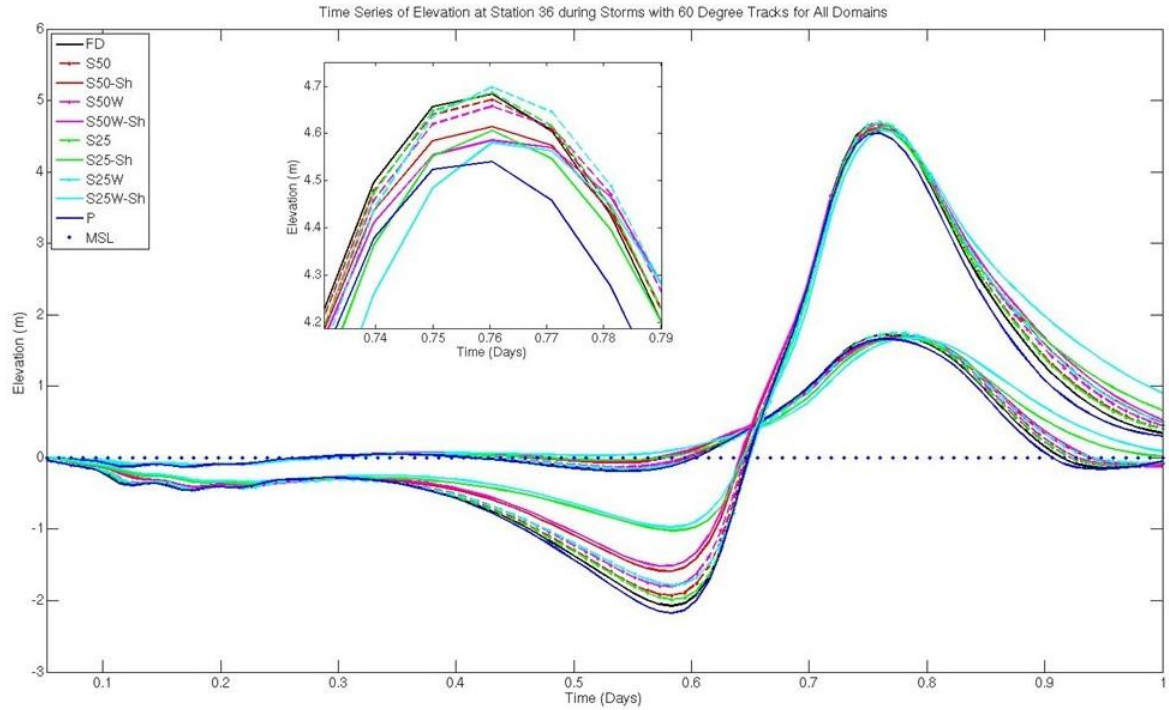

Figure 3-5: Elevation in all domains at Recording Station 36 during storms with 60° tracks, with inset showing peak elevation in each domain during the smaller (R_m = 42.4 km) storm. There was a delay in the arrival of peak surge in the domain with the close wide, shallow shoal (S25W-Sh) as well as a smaller delay in the arrival of peak surge in the domain with the close, shallow shoal (S25-Sh).

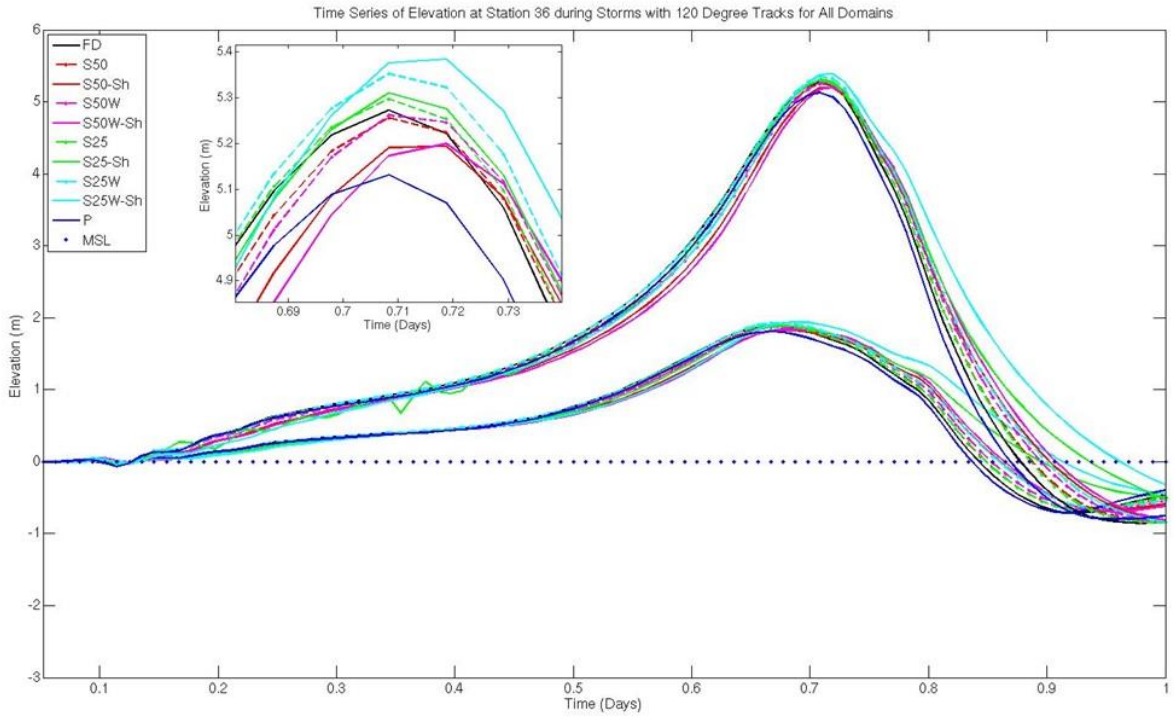

Figure 3-6: Elevation in all domains at Recording Station 36 during storms with 120° tracks, with inset showing peak elevation in each domain during the smaller (R_m = 42.4 km) storm. The domains with the distant, wide, shallow shoal (S50W-Sh) and the distant, shallow shoal (S50-Sh) experienced the largest delays in the arrival of peak surge at Station 36.

3.2.2.2. Impact of Bathymetry Features on Peak Elevation

The presence of the features did not have much impact on peak elevations at Recording Station 36. The greatest percent increase in peak surge from the featureless reference domain (FD), 4.15%, occurred in the domain with the close, wide, shallow shoal (S25W-Sh), during the large storm with the shore-normal (90°) approach (Table 3-3). The greatest percent decrease in peak surge from the FD, -4.15%, occurred in the domain with the pit (P) during the large storm approaching from the southwest (120° track) (Table 3-3).

Similarly, Weaver and Slinn (2010) found that local changes to the continental shelf bathymetry did not meaningfully impact peak surge. When they applied perturbations to the bathymetry in their 2-D simulations, the majority of their peak elevations were within ± 2% of those of the unperturbed bathymetries. In our study, peak surge levels at Recording Station 36, in domains containing features, were within ± 4.15% of the featureless reference domain's surge level under identical storm conditions (Table 3-2). This appears to be reasonable since the features used herein were a much larger departure from the surrounding seafloor than those used by Weaver and Slinn.

Table 3-3: Comparison of peak elevation in each domain with a feature to peak elevation in the featureless reference domain (FD). The comparison was done for all domains and for every storm. Elevations were taken at the recording station. Elevation differences (blue columns) are in centimeters, and percent change (white columns) is calculated according to Equation 2-10. The largest percent change from the FD is highlighted.

Difference from Elevation of Featureless Reference Domain (Peak Surge)												
Storm →	60.0 km 60° Track		60.0 km 90° Track		60.0 km 120° Track		42.4 km 60° Track		42.4 km 90° Track		42.4 km 120° Track	
Domain	Elevation Difference (cm)	Percent Change from FD	Elevation Difference (cm)	Percent Change from FD	Elevation Difference (cm)	Percent Change from FD	Elevation Difference (cm)	Percent Change from FD	Elevation Difference (cm)	Percent Change from FD	Elevation Difference (cm)	Percent Change from FD
S50	0.34	0.20%	1.93	1.11%	-1.54	-0.82%	-1.14	-0.24%	2.18	0.44%	-1.64	-0.31%
S50W	0.76	0.44%	5.17	2.98%	-0.79	-0.42%	-2.54	-0.54%	6.78	1.38%	-1.08	-0.20%
S50-Sh	-2.97	-1.73%	3.19	1.84%	-5.51	-2.93%	-6.85	-1.46%	1.88	0.38%	-7.91	-1.50%
S50W-Sh	-1.95	-1.13%	5.95	3.43%	-4.31	-2.29%	-9.75	-2.08%	5.79	1.18%	-7.30	-1.38%
S25	0.87	0.51%	1.33	0.77%	1.22	0.65%	0.31	0.07%	2.98	0.61%	2.48	0.47%
S25W	2.51	1.46%	4.09	2.36%	4.58	2.43%	1.43	0.31%	9.57	1.94%	8.00	1.52%
S25-Sh	-5.06	-2.94%	2.58	1.49%	0.53	0.28%	-7.66	-1.64%	5.21	1.06%	3.77	0.72%
S25W-Sh	-5.18	-3.01%	7.20	4.15%	5.53	2.94%	-10.24	-2.19%	16.71	3.39%	11.24	2.13%
P	-6.12	-3.56%	-6.04	-3.48%	-7.82	-4.15%	-14.28	-3.05%	-14.79	-3.00%	-14.12	-2.68%

3.2.2.3. Impact of Bathymetry Features on Arrival of Peak Surge

One effect that some features had on peak surge was that their presence caused a small delay in its arrival during the storms that had oblique (60° and 120°) tracks. During storms with 60° tracks, domains with shallow shoals 25 km from shore experienced a small delay in the arrival of peak surge at Recording Station 36 (Fig. 3-7). The shoals' capacity to delay the arrival of surge at Station 36 was made possible by the relatively low water levels near the shoals. For the smaller, more intense storm, the cause of the low water levels was setdown due to sustained offshore winds before landfall. For the larger storm, the elevations were relatively low (less than two meters) throughout the entire passage of the storm due to its low intensity. Elevation and water velocity one half hour before landfall of the small storm is shown in Fig. 3-8. (Fig. 3-9 depicts the same for large storm.) In these snapshots, which show water levels just prior to peak surge, a small depression in elevation at Station 36 is visible in the domain with the close, wide, shallow shoal compared with the elevation in the FD. Before the elevation grew deeper as the storms neared landfall, the close, shallow shoals (especially the wide one, S25W-Sh) delayed movement of the water shoreward, towards Station 36 (Figure 3-7), but this effect only lasted until the water levels increased, inundating the shoals and allowing water to flow unimpeded over them. Peak surge in the domain with the close, wide, shallow shoal (S25W-Sh) during the small storm approaching from the southeast was less than in the reference domain by 10.24 cm, but this was only a change of -2.19% (Table 3-3).

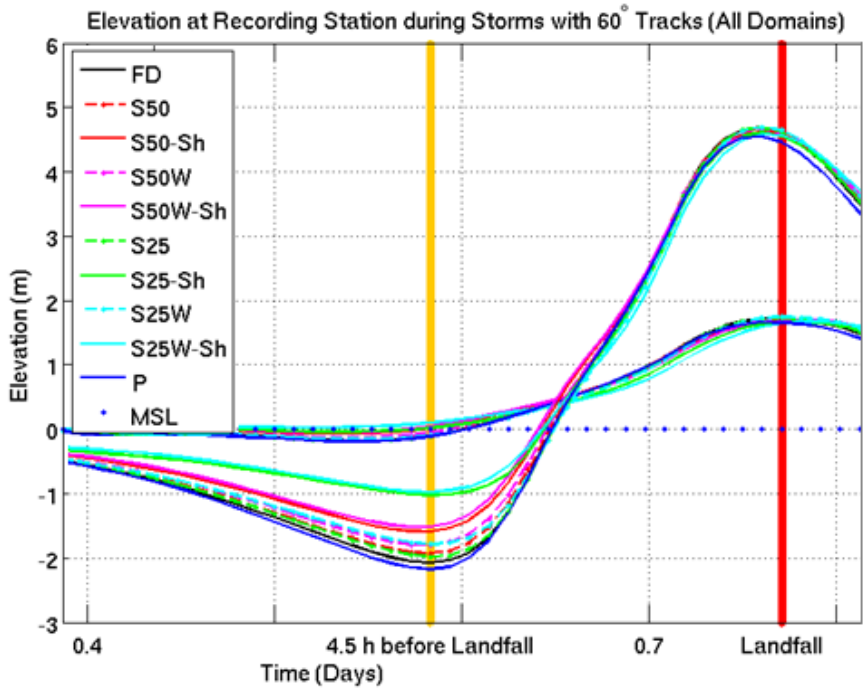

Figure 3-7: Delay in the arrival of surge at Station 36 during the storms approaching from the southeast (60° track). In the smaller (R_m = 42.4 km) storm (highest curve), a small delay in the arrival of peak surge in the domain with the close, wide, shallow shoal (S25W-Sh) is visible as is a smaller delay in the arrival of peak surge in the domain with the close, shallow shoal (S25-Sh). The delay in the arrival of peak surge in these domains is more prominent during the larger (R_m = 60.0 km) storm in which water levels were lower.

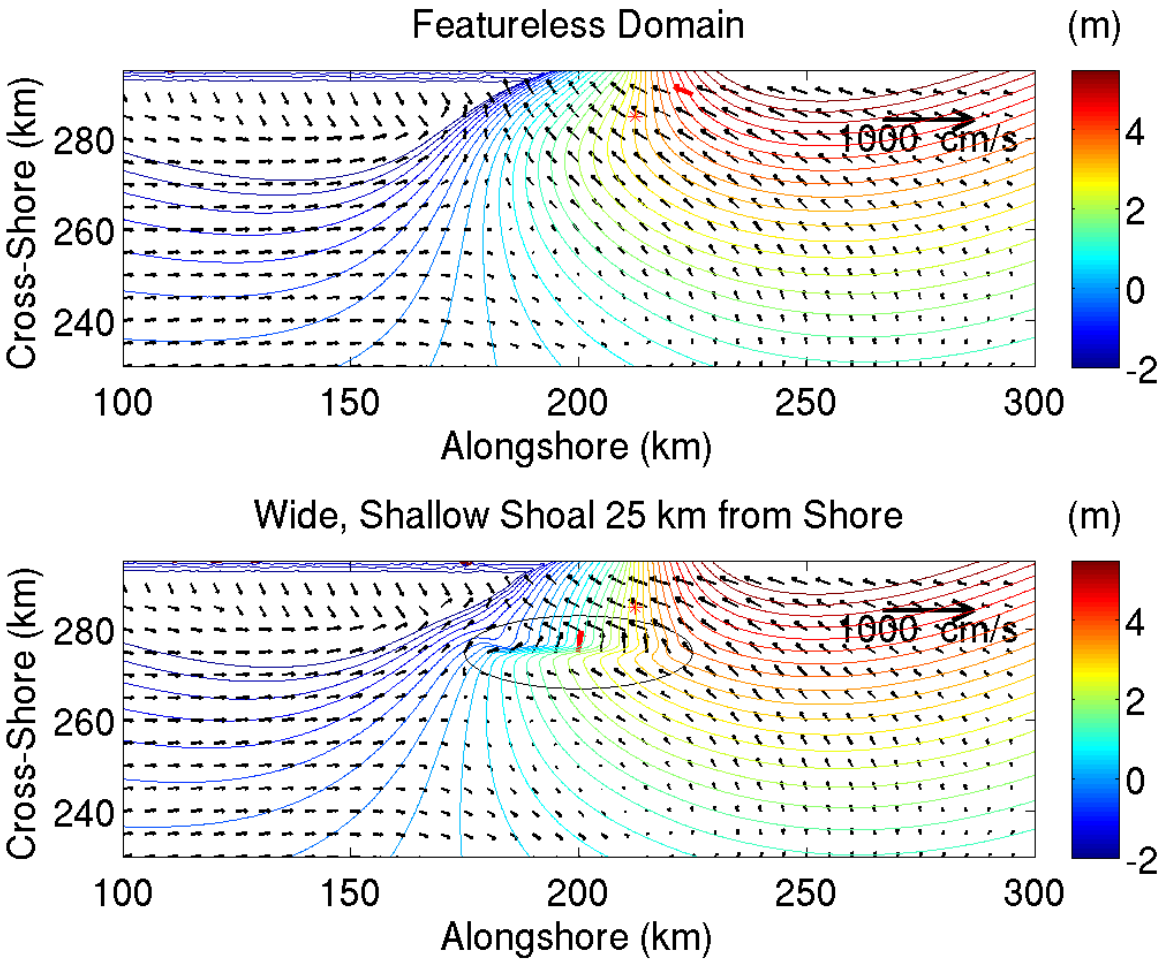

Figure 3-8: Elevation and water velocity one half hour before landfall in the featureless reference domain (FD) and in the domain with the wide, shallow shoal 25 km from shore (S25W-Sh), during the smaller (42.4 km R_m), more intense storm approaching from the southeast (60° track). Shore is located 5 km above each plot. The red asterisk in each plot shows the location of Station 36. Elevation is indicated by colored contour lines, and water velocity is indicated by arrows. Sustained offshore winds caused setdown, visible on the left side of each plot. Before the water levels increased to the point of inundating the wide, shallow shoal 25 km from shore, the shoal delayed the shoreward movement of water. Ultimately, this did not meaningfully impact the maximum water levels reached at Station 36 in this domain.

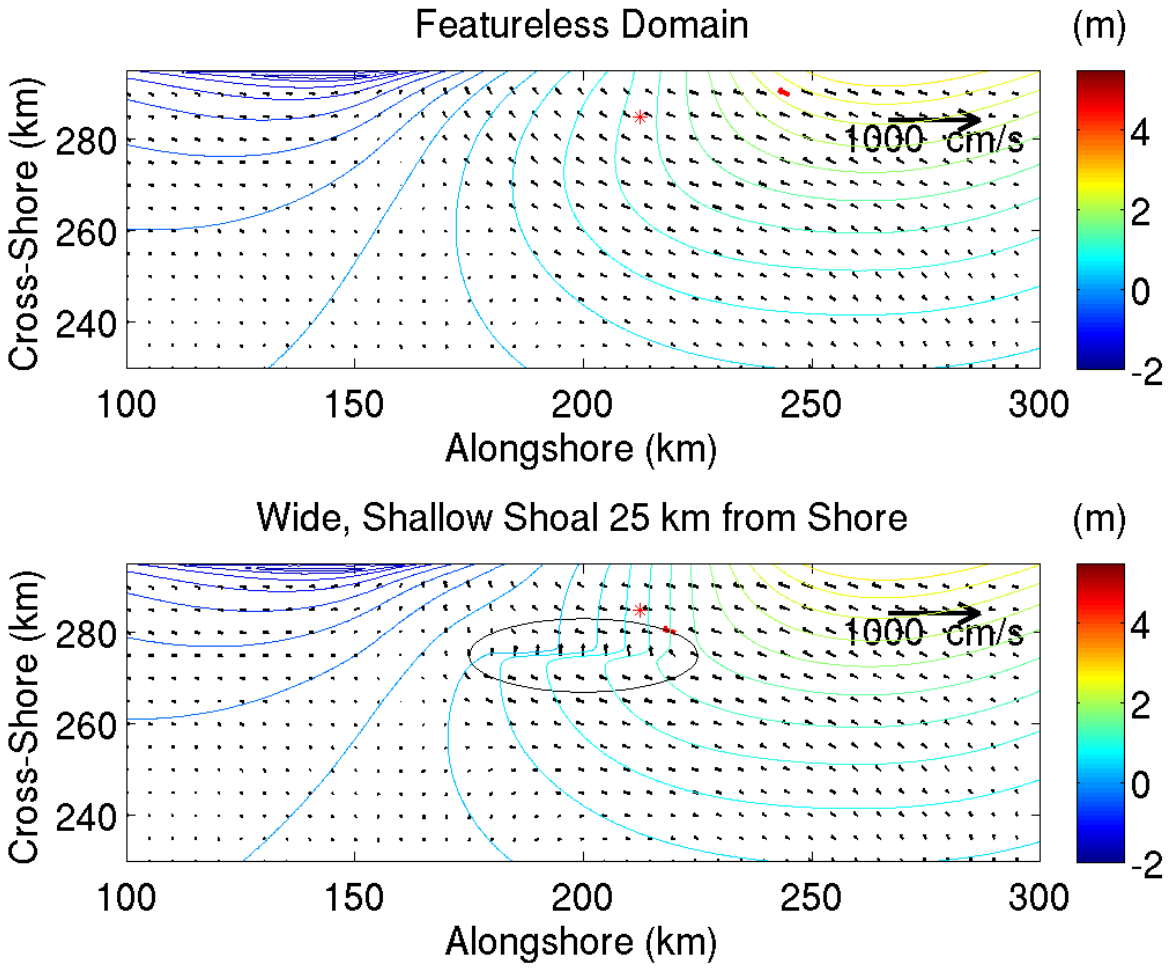

Figure 3-9: Elevation and water velocity one half hour before landfall in the featureless reference domain (FD) and in the domain with the wide, shallow shoal 25 km from shore (S25W-Sh), during the larger (60.0 km R_m), less intense storm approaching from the southeast (60° track). Shore is located 5 km above each plot. The red asterisk in each plot shows the location of Station 36. Elevation is indicated by colored contour lines, and water velocity is indicated by arrows. Sustained offshore winds caused a small amount of setdown, visible on the left side of each plot. Overall, water levels were low throughout the passage of this storm. Before the water levels increased to the point of inundating the wide, shallow shoal 25 km from shore, it delayed the shoreward movement of water, but this was not ultimately very influential to the maximum water levels reached at Station 36 in this domain.

Similarly, during storms with 120° tracks, domains with shallow shoals 50 km from shore experienced a small delay in the arrival of peak surge at Recording Station 36 (Fig. 3-10). Peak surge for storms approaching from the southwest occurred earlier relative to landfall than during the storms with other tracks due to the sustained onshore winds that occurred prior to landfall during these storms. Because of those onshore winds, setup occurred on the offshore sides of the shoals. The shielding effect of these shoals, particularly the shallow shoals 50 km from shore, kept elevation at Station 36 slightly depressed until it was overwhelmed by the increasing depth of the water. Pictured in Figure 3-11 (top) is the elevation at Station 36 in the featureless reference domain (FD) and (bottom) in the domain with the wide, shallow shoal 50 km from shore (S50W-Sh) 2.5 hour before landfall of the smaller, more intense storm. The difference in

elevation in the two domains at Station 36 is visible. Also visible is the setup on the offshore side of the shoal that was caused by the sustained onshore winds. The onshore direction of the wind stress that caused the aforementioned shoaling is shown in Figure 3-12. Peak surge in the domain with the distant, wide, shallow shoal (S50W-Sh) during the smaller, more intense storm was ultimately 7.30 cm less than in the reference domain, but this is only a change of -1.38% (Table 3-3). Overall, peak surge elevations and time of peak surge were largely unaffected by the features considered.

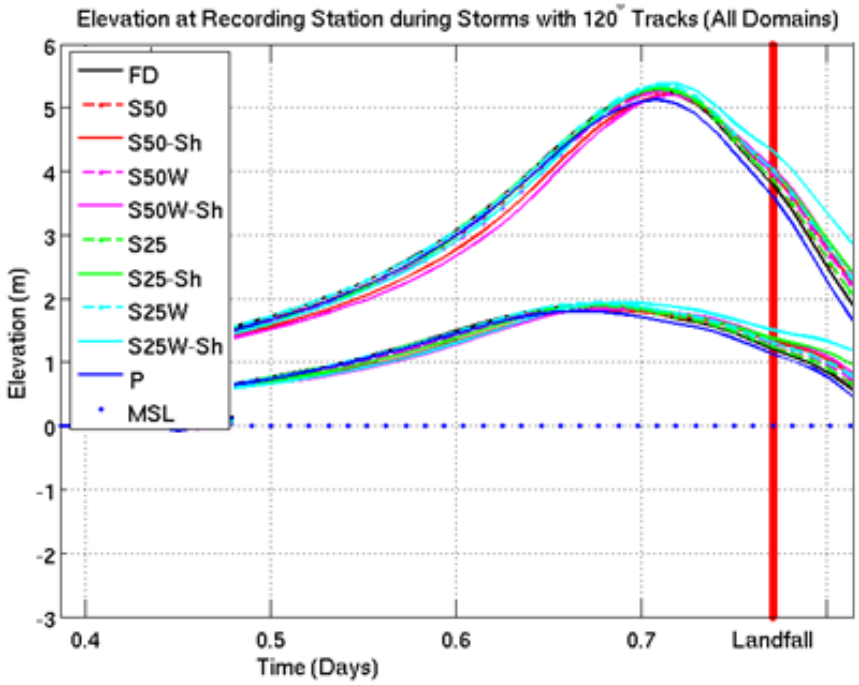

Figure 3-10: Delay in the arrival of surge at Station 36 during the storms (R_m = 42.4 km) approaching from the southwest (120° track). The most noticeable delay is during the smaller, more intense storm (highest curve) in the domains with distant, shallow shoals (S50W-Sh and S50-Sh).

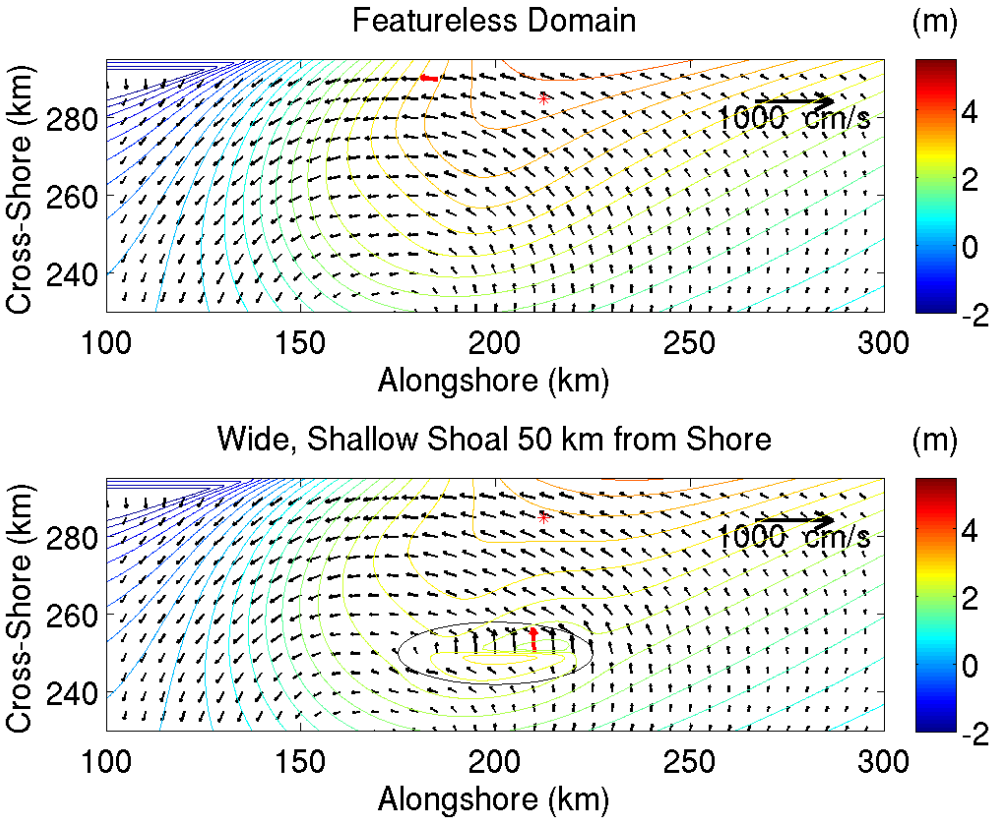

Figure 3-11: Elevation and water velocity 2.5 hours before landfall in the featureless reference domain (FD) and the domain with the wide, shallow shoal 50 km from shore (S50W-Sh), during the smaller (42.4 km R_m), more intense storm approaching from the southwest (120° track). Shore is located 5 km above each plot. The red asterisk in each plot shows the location of Station 36. Elevation is indicated by colored contour lines, and water velocity is indicated by arrows. This storm track caused sustained onshore winds, and setup is visible on the offshore side of the shoal. The presence of the feature keeps the elevation at Station 36 slightly depressed until the influence of the local bathymetry is overwhelmed by the increasing wind stress and water depth.

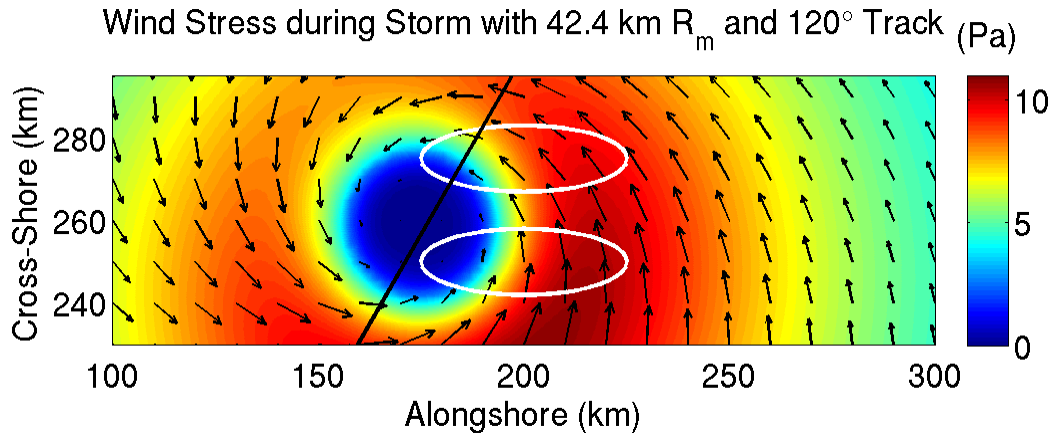

Figure 3-12: Wind stress 2.5 hours before landfall of the small storm (R_m = 42.4 km) approaching from the southwest (120° Track). Wind stress magnitude is indicated by color, and arrows indicate both the magnitude and direction. Shore is located 5 km above plot. The red asterisk shows the location of Station 36. The locations of the wide features at each distance from shore (25 and 50 km) are shown using white outlines. The storm track is shown as a black line. Onshore winds caused shoaling on the offshore side of the shoals. This caused a delay in the arrival of peak surge in the domains with shallow shoals 50 km from shore.

3.3. Effect of Bathymetry Features on Surge 3 Hours after Landfall

After conducting the same initial analyses on elevations three hours after the storms made landfall (Table 3-4) as during the time of peak surge, it was clear that the bathymetry features did influence surge generation at this time. The difference in centimeters between elevation in each domain with a feature and the featureless reference domain (FD) as well as the percent change in elevation from the FD for each domain can be found in Table 3-5. Of all times at which surge was examined at Station 36, only after the storms made landfall did the bathymetry features effect surge under all storm conditions. This is visible in the elevation time series at Station 36 during all six storms (Figure 3-13). Thus, at three hours after landfall the surge response to bathymetry features can be compared under all storm conditions considered.

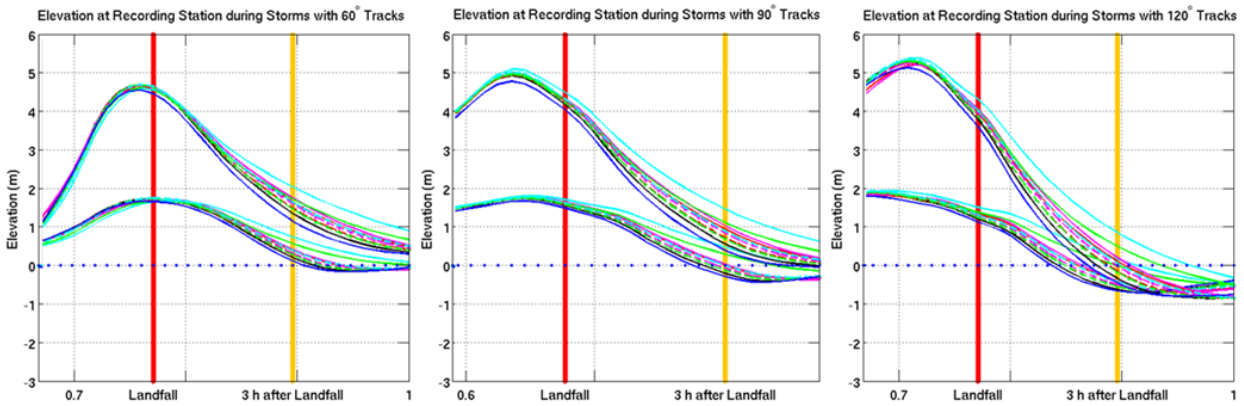

Figure 3-13: Surge response at Station 36 three hours after landfall in all domains during all six storms. The legend (not shown) is the same as in Figures 3-1, 3-2, and 3-3. The left plot shows the surge response to storms approaching from the southeast (60° track). The center plot shows the surge response to storms with a shore-normal approach (90° track). The right plot shows the surge response to storms approaching from the southwest (120° track). Three hours after landfall is indicated by a gold vertical line in each plot. The difference in elevation between the simulations that is visible three hours after the storms made landfall increases with increasing track angle and is most prominent in the domains with close, shallow shoals.

Table 3-4: Elevation (meters) at Recording Station 36 in each domain three hours after each storm has made landfall.

Elevation 3 Hours after Landfall (m)						
Domain	60.0 km 60° Track	60.0 km 90° Track	60.0 km 120° Track	42.4 km 60° Track	42.4 km 90° Track	42.4 km 120° Track
FD	0.2061	-0.2060	-0.6249	1.3534	0.5574	-0.3357
S50	0.2678	-0.1260	-0.5489	1.4863	0.7212	-0.1509
S50W	0.3170	-0.0777	-0.5037	1.5965	0.8379	-0.0204
S50-Sh	0.3859	0.0026	-0.4218	1.6558	0.9364	0.1085
S50W-Sh	0.4223	0.0308	-0.3997	1.7456	1.0256	0.2024
S25	0.2763	-0.1251	-0.5486	1.4639	0.6823	-0.1823
S25W	0.3888	0.0012	-0.4242	1.6465	0.8880	0.0639
S25-Sh	0.5665	0.2912	-0.0077	1.7250	1.1066	0.4959
S25W-Sh	0.7436	0.4704	0.1695	2.0355	1.4568	0.8527
P	0.1162	-0.2850	-0.6576	1.1530	0.3908	-0.4571

Table 3-5: Comparison of elevation three hours after landfall in each domain with a feature to peak elevation in the featureless reference domain. The comparison was done for all domains and for every storm. Elevations were taken at Recording Station 36. Elevation differences (blue columns) are in centimeters, and percent change (white columns) is calculated according to Equation 2-10. The largest percent change from the featureless reference domain (FD) is highlighted.

Difference from Elevation of Featureless Reference Domain (3 Hours after Landfall)												
Storm →	60.0 km 60° Track		60.0 km 90° Track		60.0 km 120° Track		42.4 km 60° Track		42.4 km 90° Track		42.4 km 120° Track	
Domain	Elevation Difference (cm)	Percent Change from FD	Elevation Difference (cm)	Percent Change from FD	Elevation Difference (cm)	Percent Change from FD	Elevation Difference (cm)	Percent Change from FD	Elevation Difference (cm)	Percent Change from FD	Elevation Difference (cm)	Percent Change from FD
S50	6.17	29.94%	8.00	38.83%	7.60	12.16%	13.29	9.82%	16.38	29.39%	18.48	55.05%
S50W	11.09	53.81%	12.83	62.28%	12.12	19.40%	24.31	17.96%	28.05	50.32%	31.53	93.92%
S50-Sh	17.98	87.24%	20.86	101.26%	20.31	32.50%	30.24	22.34%	37.90	67.99%	44.42	132.32%
S50W-Sh	21.62	104.90%	23.68	114.95%	22.52	36.04%	39.22	28.98%	46.82	84.00%	53.81	160.29%
S25	7.02	34.06%	8.09	39.27%	7.63	12.21%	11.05	8.16%	12.49	22.41%	15.34	45.70%
S25W	18.27	88.65%	20.72	100.58%	20.07	32.12%	29.31	21.66%	33.06	59.31%	39.96	119.03%
S25-Sh	36.04	174.87%	49.72	241.36%	61.72	98.77%	37.16	27.46%	54.92	98.53%	83.16	247.72%
S25W-Sh	53.75	260.80%	67.64	328.35%	79.44	127.12%	68.21	50.40%	89.94	161.36%	118.84	354.01%
P	-8.99	-43.62%	-7.90	-38.35%	-3.27	-5.23%	-20.04	-14.81%	-16.66	-29.89%	-12.14	-36.16%

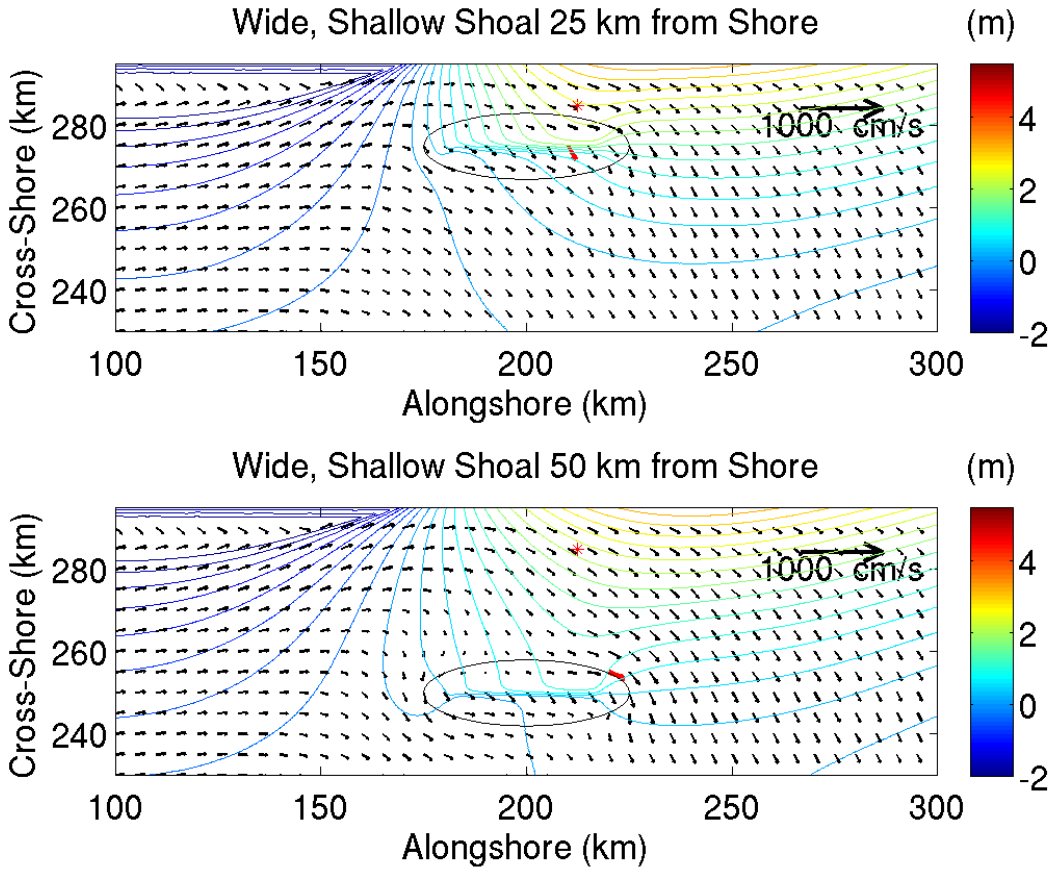

Figure 3-14: Elevation and water velocity 3 hours after landfall in the domains with the wide, shallow shoal at each distance from shore (S25W-Sh and S50W-Sh), during the smaller (42.4 km R_m), more intense storm with a shore-normal approach (90° track). Shore is located 5 km above each plot. The red asterisk in each plot shows the location of Station 36. Elevation is indicated by colored contour lines and water velocity is indicated by arrows. The contours show the shoaling that occurred on the nearshore sides of the shoals during the recession of the storm surge. This occurred under all storm conditions.

The surge response after landfall, shoaling on the nearshore side of the shoals (Figure 3-14), was a result of water that had built up near shore returning offshore, predominantly under the force of gravity. Examination of the wind stress direction at this time, for all storms (not shown), ruled out wind stress as the driver of the aforementioned shoaling during surge recession.

3.3.1. Surge Response to Shoals by Feature Class

After showing that the features did influence elevation during surge recession and that the various features influenced surge to differing extents, the features' influence on surge generation was evaluated by feature (shoal) class. Since surge generation is inversely proportional to water depth, it was expected that shallow features would cause more surge generation than deeper features that were otherwise the same (i.e. having the same cross-shore width and distance from shore). Similarly, it was expected that wide features would cause greater surge generation than narrow features that were otherwise the same (i.e. having the same depth below MSL and distance from shore) because there is a larger area having shallower depths in the case of the wide features than in the case of the narrower features, thus increasing surge generation. Because surge is also inversely proportional to bottom slope, close features were expected to cause greater surge generation than analogous features (i.e. those having the same depth below MSL and same cross-shore width) located farther from shore. This is due to the fact that in order for the more distant features, which are located in deeper water, to have the same depth below MSL and same cross-shore width as the closer features, they must have more steeply sloped sides thereby causing less surge generation. This pattern of shallow features being more influential than deep ones, wide features more influential than narrow ones, and close features more influential than distant ones was consistent under all storm conditions tested. Under all conditions, shallow shoals were the most influential class of features on surge generation, and deep shoals were the least influential. Though narrow features were never more influential than wide ones nor were distant features more influential than close ones, the order of influence between wide features and close features (and between narrow features and distant ones) varied based on storm conditions. The most common order of influence was the one reflected in the mean results shown in Table 3-6.

Table 3-6: Influence of shoal class on surge generation three hours after landfall (mean results for all six storms).

Mean Shoal Influence by Class on Surge 3 Hours after Landfall		
Order of Class Influence on Surge Generation (All 6 Storms)	Class Name	Mean Change (cm) from FD by Class (All 6 Storms)
0.5 m below MSL	Shallow Features	49.16
25 km from shore	Close Features	42.65
11.25 km wide	Wide Features	40.28
3.75 km wide	Narrow Features	26.08
50 km from shore	Distant Features	23.72
3.0 m below MSL	Deep Features	17.20

3.3.2. Surge Response to Features Analyzed by Storm Size

When the surge response was analyzed by storm size, the order of influence by feature class differed for storms of different sizes. The order of influence during the larger, less intense storms was the same as that reflected in the mean results. Though the wide features became more influential on surge generation than the close features during the smaller (42.4 km R_m), more intense storms, the two categories were nearly equal in influence. There was less than a one centimeter difference in the surge response to the wide features and the response to close features. These values are shown in peach in Table 3-6. Similarly, although the distant features were more influential than the narrow features in the case of the small storms, the difference was also less than a centimeter. These values are shown in blue in Table 3-7.

Table 3-7: Influence of shoal class on surge generation three hours after landfall analyzed by storm size. This table shows the mean results for storms of each size: R_m = 60.0 km and R_m = 42.4 km. During the 42.4 km storms, the order of class influence differed from the mean (and most common) order. Notice that though the wide features were more influential than the close features, the wide features and the close features (shaded peach) were nearly equal in their influence. Similarly, although the distant features were more influential than the narrow features (both shaded blue), they were nearly identical in their influence.

Shoal Influence by Class on Surge 3 Hours after Landfall - Analyzed by Storm Size			
Order of Class Influence on Surge Generation (60.0 km Storms)	Mean Change (cm) from FD by Class (60.0 km Storms)	Order of Class Influence on Surge Generation (42.4 km Storms)	Mean Change (cm) from FD by Class (42.4 km Storms)
0.5 m below MSL	39.61	0.5 m below MSL	58.72
25 km from shore	35.84	11.25 km wide	50.26
11.25 km wide	30.31	25 km from shore	49.45
3.75 km wide	20.93	50 km from shore	32.04
50 km from shore	15.40	3.75 km wide	31.24
3.0 m below MSL	11.63	3.0 m below MSL	22.77

3.3.3. Surge Response to Features Analyzed by Storm Track

For two of the three storm tracks, the feature classes had the same order of influence on surge generation as reflected by the mean values in Table 3-6. It was only during storms approaching from the southeast (60° track) that there was a departure from the typical order. Just as when the elevations were evaluated by storm size, in the case where there was a different order of influence, the wide features became more influential on surge generation than the close features, and, again, the influence of the two shoal classes was nearly identical with less than a centimeter difference in elevation between the domains with wide features and the domains with close features. These values are shown in peach in Table 3-8. Again, the distant features were more influential than the narrow features, and the difference in elevation between the domains with distant features and those with narrow features was also less than a centimeter. These values are shown in blue in Table 3-8.

Table 3-8: Influence of shoal class on surge generation three hours after landfall analyzed by storm track. This table shows the mean results for storms with each track: 60°, 90°, and 120°. During the storms with 60° tracks, the order of class influence differed from the mean (and most common) order. Notice that though the wide features were more influential than the close features, the wide features and the close features (shaded peach) were nearly equal in their influence. Similarly, although the distant features were more influential than the narrow features (both shaded blue), they were nearly identical in their influence.

Shoal Influence by Class on Surge 3 Hours after Landfall - Analyzed by Storm Track					
Order of Class Influence on Surge Generation (60 Degree Storms)	Mean Change (cm) from FD by Class (60 Degree Storms)	Order of Class Influence on Surge Generation (90 Degree Storms)	Mean Change (cm) from FD by Class (90 Degree Storms)	Order of Class Influence on Surge Generation (120 Degree Storms)	Mean Change (cm) from FD by Class (120 Degree Storms)
0.5 m below MSL	38.03	0.5 m below MSL	48.94	0.5 m below MSL	60.53
11.25 km wide	33.22	25 km from shore	42.07	25 km from shore	53.27
25 km from shore	32.60	11.25 km wide	40.34	11.25 km wide	47.29
50 km from shore	20.49	3.75 km wide	26.05	3.75 km wide	32.33
3.75 km wide	19.87	50 km from shore	24.32	50 km from shore	26.35
3.0 m below MSL	15.06	3.0 m below MSL	17.45	3.0 m below MSL	19.09

3.3.4. Surge Response to Features Analyzed by Individual Storm

In order to better understand the cause of the differing surge responses to the feature classes during storms with different sizes and tracks, feature influence by class was analyzed for each storm. When analyzing shoal influence by feature class for each individual storm, it became apparent that there was a single storm (42.4 km R_m with a 60° track) with a strong atypical response (shaded peach and blue in Table 3-8) and a second storm (42.4 km R_m with a 90° track) with a similar, though weaker response (shaded pale peach and pale blue in Table 3-8). In the storm with the largest departure from the typical order of feature class influence (42.4 km R_m with a 60° track), the domains with wide shoals had a 3.83 cm higher mean elevation than the domains with close shoals (and the domains with distant shoals had the same increase in mean elevation over the domains with narrow shoals). In the case of the storm with the smaller deviation from the typical order of class influence (42.4 km R_m with a 90° track), the domains with wide shoals had a mean elevation 1.87 cm higher than in the domains with close shoals. Again, the domains with distant shoals had the same increase in mean elevation over the domains with narrow shoals. Given that the results grouped by storm track contained the mean of only two storms per track, the influence of the storm with the strongest response, which had greater elevations than the 60.0 km storm with the same track, was sufficient to determine the order of class influence for storms with 60° tracks. Both storms with the atypical response had R_m = 42.4 km so it is understandable that comprising two thirds of the storms of that size category, they could determine the order of class influence for the smaller (42.4 km R_m) storms.

Table 3-9: Influence of shoal class on surge generation three hours after landfall analyzed by individual storm. This table shows the order of feature class influence on surge 3 hours after each storm has made landfall. There were two storms with an atypical order of influence of the feature classes. The largest departures from the typical order are shaded in peach and blue. The smaller departures are shaded in pale peach and pale blue.

Shoal Influence by Class on Storm Surge 3 Hours after Landfall - Analyzed by Storm					
60° Track		**90° Track**		**120° Track**	
60.0 km RMW		**60.0 km RMW**		**60.0 km RMW**	
Order of Class Influence on Surge Generation 60.0 km 60° Track	Mean Change (cm) from FD by Class 60.0 km 60° Track	Order of Class Influence on Surge Generation 60.0 km 90° Track	Mean Change (cm) from FD by Class 60.0 km 90° Track	Order of Class Influence on Surge Generation 60.0 km 120° Track	Mean Change (cm) from FD by Class 60.0 km 120° Track
0.5 m below MSL	32.35	0.5 m below MSL	40.48	0.5 m below MSL	46.00
25 km from shore	28.77	25 km from shore	36.54	25 km from shore	42.22
11.25 km wide	26.18	11.25 km wide	31.22	11.25 km wide	33.54
3.75 km wide	16.80	3.75 km wide	21.67	3.75 km wide	24.32
50 km from shore	14.22	50 km from shore	16.34	50 km from shore	15.64
3.0 m below MSL	10.64	3.0 m below MSL	12.41	3.0 m below MSL	11.86
60° Track		**90° Track**		**120° Track**	
42.4 km RMW		**42.4 km RMW**		**42.4 km RMW**	
Order of Class Influence on Surge Generation 42.4 km 60° Track	Mean Change (cm) from FD by Class 42.4 km 60° Track	Order of Class Influence on Surge Generation 42.4 km 90° Track	Mean Change (cm) from FD by Class 42.4 km 90° Track	Order of Class Influence on Surge Generation 42.4 km 120° Track	Mean Change (cm) from FD by Class 42.4 km 120° Track
0.5 m below MSL	43.71	0.5 m below MSL	57.40	0.5 m below MSL	75.06
11.25 km wide	40.26	11.25 km wide	49.47	25 km from shore	64.33
25 km from shore	36.43	25 km from shore	47.60	11.25 km wide	61.04
50 km from shore	26.77	50 km from shore	32.29	3.75 km wide	40.35
3.75 km wide	22.94	3.75 km wide	30.42	50 km from shore	37.06
3.0 m below MSL	19.49	3.0 m below MSL	22.50	3.0 m below MSL	26.33

3.3.4.1. Analysis of Atypical Order of Feature Class Influence

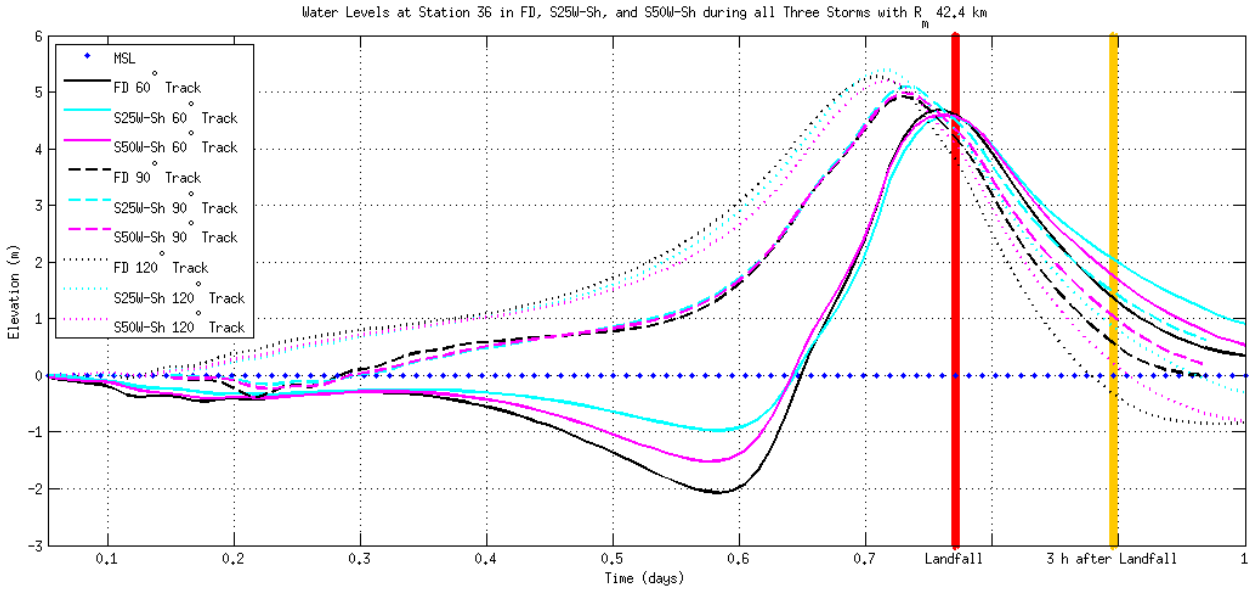

Figure 3-15: Water levels at Station 36 in the featureless reference domain (FD) and the domains with the most influential shoal at each distance from shore (S25W-Sh and S50W-Sh), during all three smaller (42.4 km R_m), more intense storms. Though all storms had the same forward speed, the storm with the 90° track took less time to go through the domains so its time of landfall and, by default, 3 hours after landfall have been aligned with the times they occurred in during the two oblique tracks.

The storm with the most atypical response (the small storm approaching from the southeast) had the highest water levels at 3 hours after landfall of all storms. Figure 3-15 shows the water levels in the FD, S25W-Sh, and S50W-Sh domains during the smaller storms. The average elevation in domains with shoals was 1.67 m (calculated from Table 3-4). Under these conditions, the influence of the narrow, shallow shoal 25 km from shore (S25-Sh) decreased, and the influence of the wide, shallow shoal 50 km from shore (S50W-Sh) increased. Overall, the wide features 50 km from shore were more influential on surge generation than the narrow features 25 km from shore by a margin of 3.83 cm (calculated from Table 3-9). The increase in influence of the wide features 50 km from shore relative to the narrow features 25 km from shore was also the cause for the distant features to be more influential than the narrow ones (Table 3-9). Even though the shallow features were always the most influential of the classes, it is apparent that their dominance was not as great when the water levels were relatively high, as there was only a difference of 3.45 cm between the average surge in domains with shallow features than the next most influential class, the wide features (calculated from Table 3-9). The influence of the shallow features over the next most influential class, which can vary, was larger for the other tracks, increasing with increasing track angle.

The average water level in domains with shoals during the storm with the lesser atypical response (the small storm with a shore-normal approach) was 0.96 m (calculated from Table 3-4). Again, under the conditions of elevated water levels, the wide features 50 km from shore

were more influential than the narrow features 25 km from shore. This caused the wide features to be more influential to surge generation than the close features, though with a smaller margin of 1.87 cm despite the overall surge response being larger than in the storm with a 42.4 km R_m and a 60° track. Again, the increase in influence of the wide features 50 km from shore relative to the narrow features 25 km from shore was also the cause of the distant features being more influential than the narrow ones.

3.4. Effect of Bathymetry Features on Setdown Occurring 4.5 Hours before Landfall during the Small Storm Approaching from the Southeast

Four and a half hours before the small storm approaching from the southeast (60° track) made landfall, sustained offshore winds, depicted in Figure 3-17, caused setdown to occur, but shoaling on the nearshore sides of some shoals diminished this effect (Figure 3-18). The setdown is clearly visible in the elevation time series at Station 36 (Figure 3-16). The gold vertical line indicates 4.5 hours before landfall, which is the time when elevation was examined. Since the bathymetry features affected surge generation to different extents, shoal influence was evaluated by class. The order of influence of each feature class on surge generation (Table 3-10) was the same order reflected in the mean results during surge recession (Table 3-6). Here, as during surge recession, water levels were low, and this is most likely the cause for the same order of class influence. Under these conditions, the shallow shoals close to shore were the most effective at reducing setdown at Station 36 (Table 3-11).

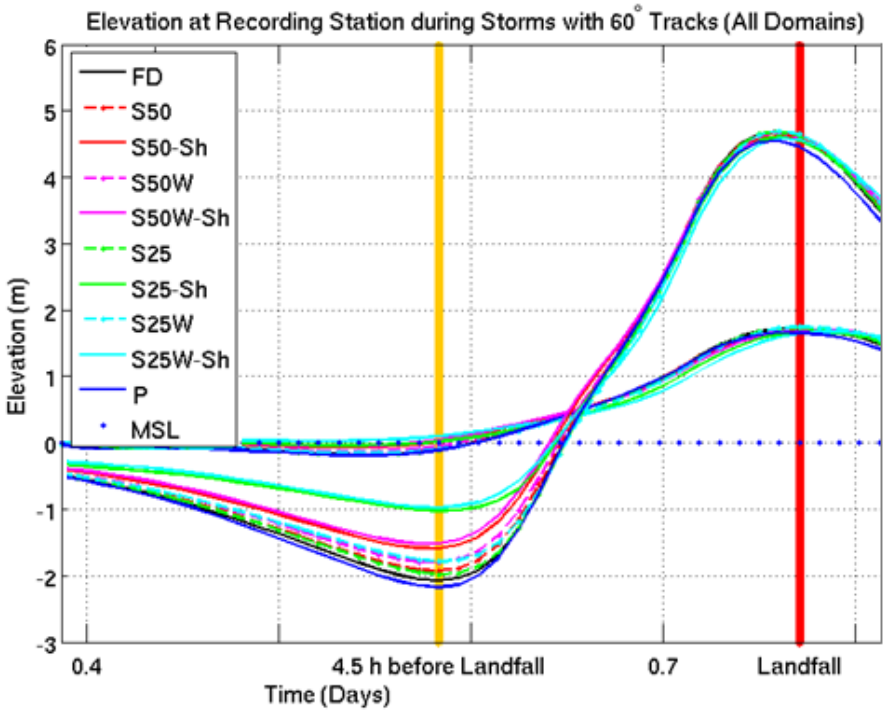

Figure 3-16: Examination of feature influence during set-down occurring 4.5 hours before landfall of the small (R_m = 42.4 km) storm approaching from the southeast (60° track). The shallow shoals, particularly those 25 km from shore, diminished the effect of the setdown at Station 36 caused by sustained offshore winds before landfall.

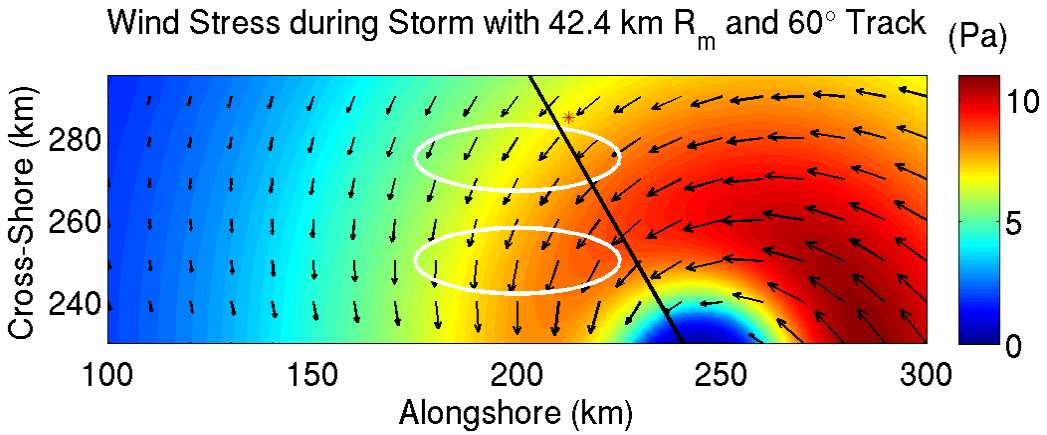

Figure 3-17: Wind stress at 4.5 hours before landfall during the storm with a 42.4 km R_m and a 60° tack. Wind stress magnitude is indicated by color, and arrows indicate both the magnitude and direction. Shore is located 5 km above plot. The red asterisk shows the location of Station 36. The locations of the wide features at each distance from shore (25 and 50 km) are shown using white outlines. The storm track is shown as a black line. The offshore winds caused setdown to occur, but shoaling on the nearshore sides of the shoals diminished this effect in some of the domains.

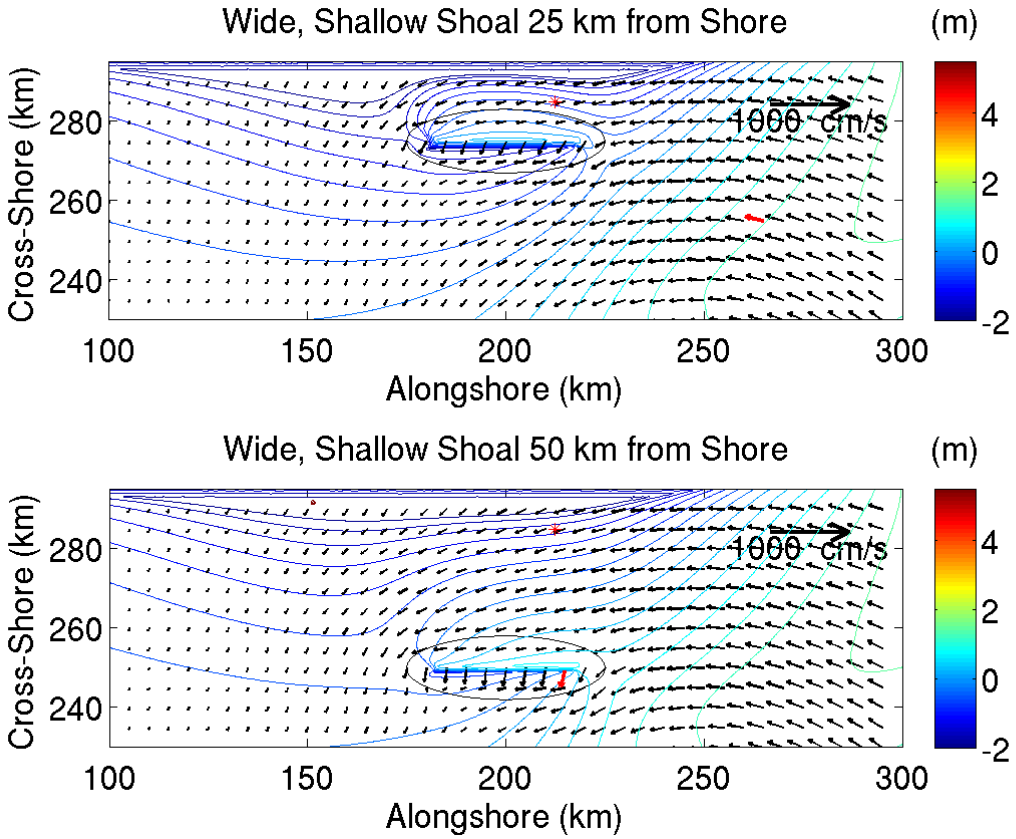

Figure 3-18: Elevation and water velocity 4.5 hours before landfall in the domains with the most influential shoal at each distance from shore (S25W-Sh and S50W-Sh), during the smaller (42.4 km R_m), more intense storm with a 60° track. Shore is located 5 km above each plot. The red asterisk in each plot shows the location of Station 36. Elevation is indicated by colored contour lines, and water velocity is indicated by arrows. Sustained offshore winds caused setdown, but the influence of these features on storm surge was made evident by the shoaling that was present on their nearshore sides.

Table 3-10: Influence of shoal class on surge generation four and a half hours before landfall during the storm with a 42.4 km R_m and a 60° track.

Shoal Influence by Class on Surge 4.5 Hours before Landfall		
Order of Class Influence on Surge Generation	Class Name	Mean Change (cm) from FD by Class
0.5 m below MSL	Shallow Features	80.08
25 km from shore	Close Features	63.55
11.25 km wide	Wide Features	55.68
3.75 km wide	Narrow Features	44.57
50 km from shore	Distant Features	36.70
3.0 m below MSL	Deep Features	20.17

Table 3-11: Metrics during the setdown that occurred at the recording station 4.5 hours before landfall during the small storm approaching from the southeast (60° track) including: 1) elevation (meters) in each domain, 2) elevation difference (centimeters) of each domain containing a feature from the reference domain (blue column), and 3) percent change in elevation of each domain with a feature from that of the featureless reference domain (FD) based on Equation 2-10.

Pre-Landfall Elevation Minimum			
Domain	**Elevation (m)**	**Diff. (cm) from FD**	**% Change. from FD**
FD	-2.0762		
S50	-1.9288	14.74	7.10%
S50W	-1.7999	27.63	13.31%
S50-Sh	-1.5878	48.84	23.52%
S50W-Sh	-1.5202	55.60	26.78%
S25	-1.9854	9.09	4.38%
S25W	-1.7838	29.24	14.08%
S25-Sh	-1.0199	105.63	50.87%
S25W-Sh	-0.9737	110.25	53.10%
P	-2.1778	-10.16	-4.89%

4. Conclusion

Numerical simulations were conducted in which ten different bathymetries were subjected to six different storms in order to determine if the features considered influenced surge generation. A range of features was considered including eight shoals, one pit, and a featureless reference domain. The storms had one of three tracks, each with a different landfall direction (60°, 90°, or 120°), and they were either one of two sizes, R_m = 42.4 or 60.0 km. The larger (60.0 km) storms were the strength of a tropical storm, and the smaller (42.4 km) storms were the strength of a Category 5 hurricane on the Saffir-Simpson scale.

The features were not impactful to peak surge or to surge at the coast, but there were certain times when the features were locally influential to surge generation, such as during surge recession and prior to peak surge. During those times when the features did influence surge generation, the individual features influenced it to varying extents. Therefore, analyses were conducted to determine which feature characteristics were most influential to surge generation and if their influence was sensitive to storm conditions.

At those times when the features were influential to surge generation, feature depth below MSL was the most impactful parameter, with shallow (0.5 m below MSL) features causing the greatest increase in elevation from the reference domain (FD) and deep features (3.0 m below MSL) causing the least. Generally, feature distance from shore was the second most impactful parameter with close (25 km from shore) features being second to the shallow features in increasing local surge. Feature cross-shore width was generally considered to be the least impactful parameter on surge generation, as the increase in surge over the FD caused by the wide features (11.25 km cross-shore width) and the increase in surge over the FD caused by the narrow features (3.75 km cross-shore width) were often the most similar of all comparisons made regarding the influence of a single parameter.

4.1. Potential Application of Findings

As previously discussed, it was determined that features such as those considered in this study do not have much impact on surge generation at the coast or on peak surge. If small-scale surge generation close to the features is not consequential to an end user, then the features do not need to be well-characterized in, or can even be omitted from, bathymetry datasets used in the creation of computational model domains without adversely impacting the outcome of simulations. This can reduce the financial resources needed to conduct high-resolution surveys characterizing continental shelf bathymetry features on the scale of those considered in this study that are greater than 25 km from shore. Additionally, it can save on computational resources needed to store and transmit such datasets, and it can maximize computational savings that result from having the bathymetry sufficiently characterized using fewer points. Furthermore, the quantification of which feature parameters influence surge and to what extent, can help inform the creation of bathymetry-thinning algorithms, allowing a developer to identify and exclude bathymetry data that does not provide additional information to the simulation of storm surge generation.

4.2. Future Work

The analyses of other stations' elevation time series could add additional insight for a few reasons. Not all instances of the features' influence on surge generation were captured by the examination of the elevation time series at Station 36. Examining these other instances, such as when setup occurred on the offshore side of the wide, shallow shoals during an onshore wind (Figure 4-1), would allow for the determination of whether the most prevalent pattern of class influence (Tables 3-6 and 3-10) discovered in this research applies to these instances as well.

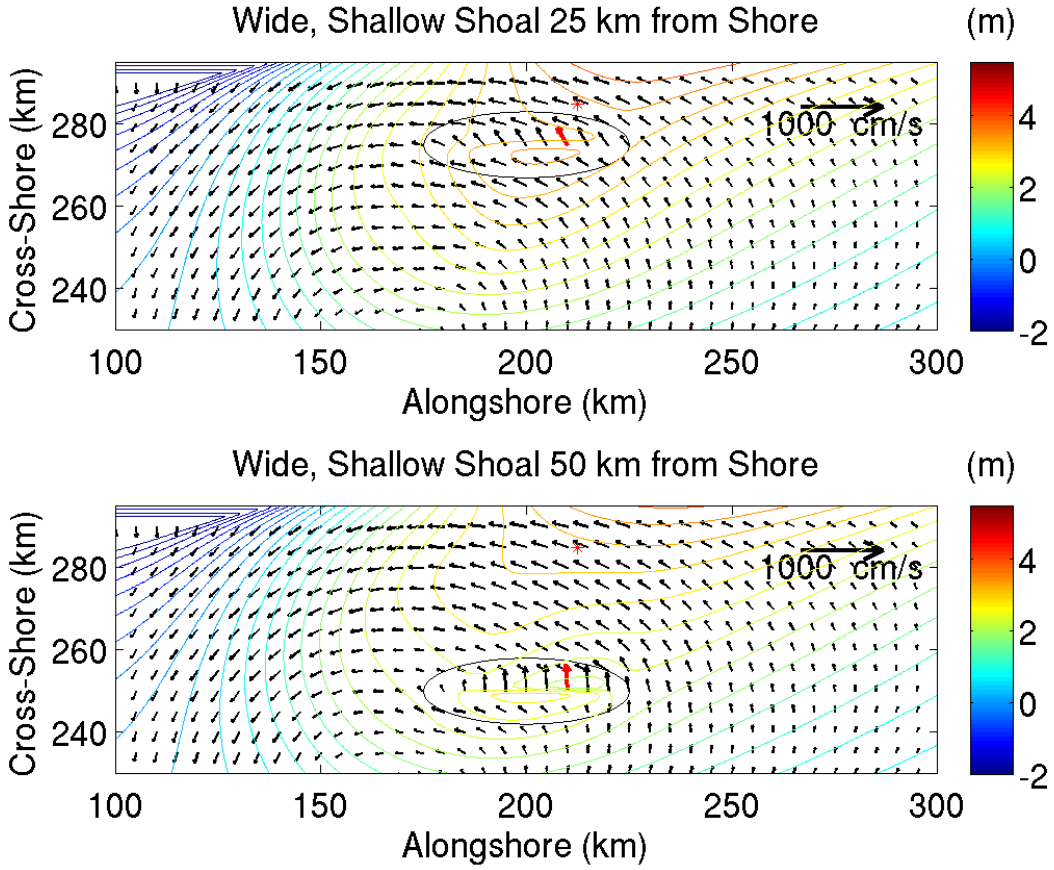

Figure 4-1: Influence of wide, shallow shoals on surge generation prior to peak surge during the small storm (R_m = 42.4 km) approaching from the southwest (120° track). Setup due to sustained onshore winds is visible on the offshore side of the shoals.

By examining surge response at a single location (Station 36), it ensured that for a given storm, the storm conditions were identical where measurements were taken, thereby not introducing any variability besides the features whose surge responses were being examined. A drawback of Recording Station 36 not being in an analogous location to the distant features (35 km shoreward of their peaks) as it was to the close features (10 km shoreward of their peaks) was that the surge response was not equally captured for both feature classes (distant features and close features). Because of Station 36's proximity to the close features, the close features'

influence on surge was well-characterized at this location. Station 36's larger distance from the distant features may have caused them to appear to be less influential to surge generation than they actually were locally. Figure 4-2 (bottom) shows that only a small amount of the surge response to the distant, wide, shallow shoal was captured by examination of elevation at Station 36.

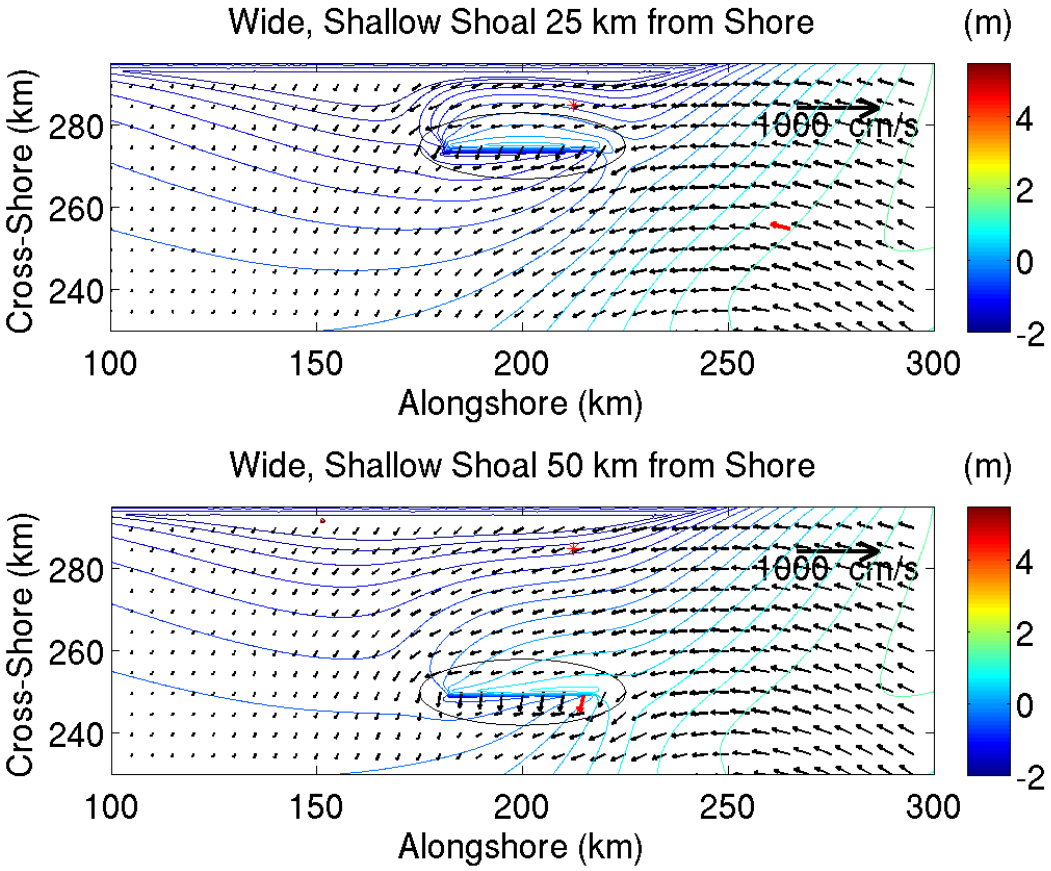

Figure 4-2: Influence of the wide, shallow shoals during the setdown that occurred 4.5 hours before landfall during the small storm (R_m = 42.4 km) approaching from the southeast (60° track). Although surge response to the distant, wide, shallow shoal was detected (bottom plot), it would be better characterized by a station in closer proximity to that shoal.

Examining elevations at two stations would allow for surge response to be analyzed the same distance from the distant features as from the close features. For example, measurements taken at Station 41 (see Figure 2-10 for Station 41's location), the station in an analogous location to the distant features as Recording Station 36 is to the close features, could show if the distant features were more influential to surge generation than they appeared to be when measurements were taken a full 35 km away from them. There could be variations in the surge at Station 41 that result from it being in a different location relative to the storm track than Station 36. Even so, it is likely that the effect of the distant features on surge that would be detected at Station 41 would be greater than any variation in surge caused by the difference in the two

stations' location relative to the storm track. Therefore, considering elevations closer to the distant shoals (i.e., at Station 41) would provide useful information about their influence on local surge generation.

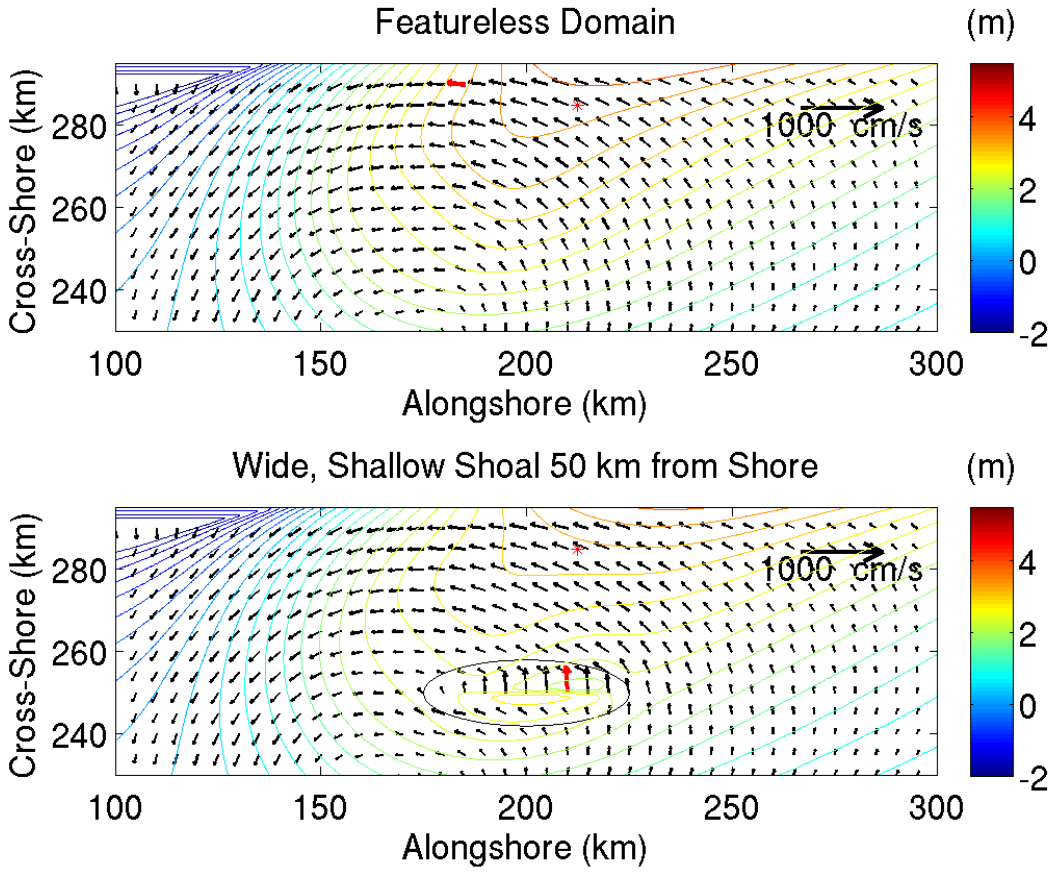

Figure 4-3: Influence of the distant, wide, shallow shoal at Station 36 prior to peak surge during the small storm (R_m = 42.4 km) approaching from the southwest (120° track).

Finally, the detection of the distant features' influence on surge at Station 36 showed that, at times, the features could influence surge some distance away from them. Figure 4-3 shows that the elevation at Station 36 differs from that of the FD when S50W-Sh is present indicating that this shoal influences surge at a location 35 km from its peak. Analyses of elevation at stations far from the features could help to further quantify the physical extent of the features' influence.

References

Atkinson, G. D., & Holliday, C. R. (1975). *Tropical Cyclone Minimum Sea Level Pressure-Maximum Sustained Wind Relationship for Western North Pacific* (No. FLEWEACEN/JTWC-TN-75-1). FLEET WEATHER CENTRAL/JOINT TYPHOON WARNING CENTER FPO SAN FRANCISCO 96630.

Blain, C. A., Linzell, R. S., Chu, P., & Massey, C. (2010). *Validation test report for the ADvanced CIRCulation Model (ADCIRC) v45. 11* (No. NRL/MR/7320-10-9205). NAVAL RESEARCH LAB STENNIS SPACE CENTER MS OCEANOGRAPHY DIV.

Blain, C. A., Linzell, R. S., & Massey, T. C. (2008). *MeshGUI: A mesh generation and editing toolset for the ADCIRC model* (No. NRL/MR/7322--08-9083). NAVAL RESEARCH LAB STENNIS SPACE CENTER MS OCEANOGRAPHY DIV.

Blain, C. A., Westerink, J. J., & Luettich, R. A. (1994). The influence of domain size on the response characteristics of a hurricane storm surge model. *Journal of Geophysical Research: Oceans (1978–2012)*, *99*(C9), 18467-18479.

Clements, B. (2009). *Disasters and public health: planning and response*. Butterworth-Heinemann.

Courant, R., Friedrichs, K., & Lewy, H. (1967). On the partial difference equations of mathematical physics. *IBM journal*, *11*(2), 215-234.

Gross, J. M., DeMaria, M., Knaff, J. A., & Sampson, C. R. (2004, May). A new method for determining tropical cyclone wind forecast probabilities. In *Preprints, 26th Conf. on Hurricanes and Tropical Meteorology, Miami, FL, Amer. Meteor. Soc. A* (Vol. 11).

Holland, G. J. (1980). An analytic model of the wind and pressure profiles in hurricanes. *Monthly weather review*, *108*(8), 1212-1218.

Irish, J. L., Resio, D. T., & Ratcliff, J. J. (2008). The influence of storm size on hurricane surge. *Journal of Physical Oceanography*, *38*(9), 2003-2013.

Kinnmark, I. P. E. (1985). *The Shallow Water Wave Equations: Formulation, Analysis, and Application* (Vol. 15, Lecture Notes in Engineering). New York, NY: Springer-Verlag.

Knaff, J. A., & Zehr, R. M. (2007). Reexamination of tropical cyclone wind-pressure relationships. *Weather and forecasting*, *22*(1), 71-88.

Li, R., Xie, L., Liu, B., & Guan, C. (2013). On the sensitivity of hurricane storm surge simulation to domain size. *Ocean Modelling*, *67*, 1-12.

Luettich, R. A., & Westerink, J. J. (1995). An assessment of flooding and drying techniques for use in the ADCIRC hydrodynamic model: Implementation and performance in one-dimensional flows. *Contract Report, prepared for Headquarters, US Army Corps of Engineers, Vicksburg, MS*.

Luettich, R. A., Westerink, J. J., & Scheffner, N. W. (1992). *ADCIRC: An Advanced Three-Dimensional Circulation Model for Shelves, Coasts, and Estuaries. Report 1. Theory and Methodology of ADCIRC-2DDI and ADCIRC-3DL* (No. CERC-TR-DRP-92-6). COASTAL ENGINEERING RESEARCH CENTER VICKSBURG MS.

Pugh, D. T. (1996). *Tides, surges and mean sea-level (reprinted with corrections)*. John Wiley & Sons Ltd.

Rego, J. L., & Li, C. (2009). On the importance of the forward speed of hurricanes in storm surge forecasting: A numerical study. *Geophysical Research Letters*, *36*(7).

Simpson, R. H., & Saffir, H. (1974). The hurricane disaster potential scale. *Weatherwise*, *27*(8), 169.

Storm Surge Overview. (n.d.) Retrieved October 11, 2016, from http://www.nhc.noaa.gov/surge

Turner, P. J. (1999, January 19). ACE/gredit online documentation. Retrieved October 05, 2016, from http://www.stccmop.org/~pturner/gredit/doc/index.html

Vickery, P. J., & Wadhera, D. (2008). Statistical models of Holland pressure profile parameter and radius to maximum winds of hurricanes from flight-level pressure and H* Wind data. *Journal of Applied Meteorology and Climatology*, *47*(10), 2497-2517.

Weaver, R. J., & Slinn, D. N. (2010). Influence of bathymetric fluctuations on coastal storm surge. *Coastal Engineering*, *57*(1), 62-70.

Webster, P. J., Holland, G. J., Curry, J. A., & Chang, H. R. (2005). Changes in tropical cyclone number, duration, and intensity in a warming environment. *Science*, *309*(5742), 1844-1846.

Wefer, G. (Ed.). (2003). *Ocean margin systems*. Springer Science & Business Media.

VITA

The author is a longtime resident of Slidell, Louisiana. She obtained her Bachelor's degrees in physics and mathematics from the University of New Orleans in 2012, graduating with university honors and honors in physics. In 2013, the author was awarded her first Naval Research Enterprise Internship Program (NREIP) internship working for Dr. Cheryl Ann Blain at the Naval Research Laboratory at Stennis Space Center, Mississippi. She continued to work as Dr. Blain's graduate research assistant through 2016. The author also obtained a Graduate Certificate in Coastal Engineering from the University of New Orleans in 2016.